Submarine karstic springs as a source of nutrients and bioactive trace metals for the oligotrophic Northwest Mediterranean Sea

Joseph Tamborski, Pieter van Beek, Pascal Conan, Mireille Pujo-Pay, Charlène Odobel, Jean-François Ghiglione, Jean-Luc Seidel, Bruno Arfib, Marc Diego-Feliu, Jordi Garcia-Orellana, et al.

Tamborski et al., 2020, Science of the Total Environment. https://doi.org/10.1016/j.scitotenv.2020.139106

Submarine karstic springs as a source of nutrients and bioactive trace metals for the oligotrophic Northwest Mediterranean Sea

Joseph Tamborski[1*^], Pieter van Beek[1], Pascal Conan[2], Mireille Pujo-Pay[2], Charlene Odobel[2], Jean-François Ghiglione[2], Jean-Luc Seidel[3], Bruno Arfib[4], Marc Diego Feliu[5], Jordi Garcia-Orellana[5,6], Armand Szafran[1], Marc Souhaut[1]

[1]LEGOS, Laboratoire d'Etudes en Géophysique et Océanographie Spatiales (Université de Toulouse, CNES, CNRS, IRD, UPS), Observatoire Midi Pyrénées, 14 Ave Edouard Belin, 31400 Toulouse, France

[2]LOMIC, Laboratoire d'Océanographie Microbienne, Observatoire Océanologique, Sorbonne Université, CNRS, UPMC Univ Paris 06, UMR7621, 66650 Banyuls/Mer, France

[3]HydroSciences Montpellier, UMR 5569 – UM2 – CNRS – IRD – UM1 Place Eugène Bataillon -CC MSE, 34095 Montpellier Cedex 5, France

[4]Aix Marseille Université, CNRS, IRD, INRAE, Coll France, CEREGE, Aix-en-Provence, France

[5]Institut de Ciència i Tecnologia Ambientals (ICTA-UAB), Universitat Autònoma de Barcelona, Bellaterra, Catalunya, Spain

[6]Department de Física, Universitat Autònoma de Barcelona, Bellaterra, Catalunya, Spain

***Correspondence:** jtamborski@whoi.edu

^Present address:

Department of Marine Chemistry and Geochemistry, Woods Hole Oceanographic Institution, Woods Hole, MA 02543 USA

Centre for Water Resources Studies, Dalhousie University, Halifax, NS, Canada

Keywords: karst; springs; submarine groundwater discharge; nutrients; radium isotopes; GEOTRACES

Graphical Abstract

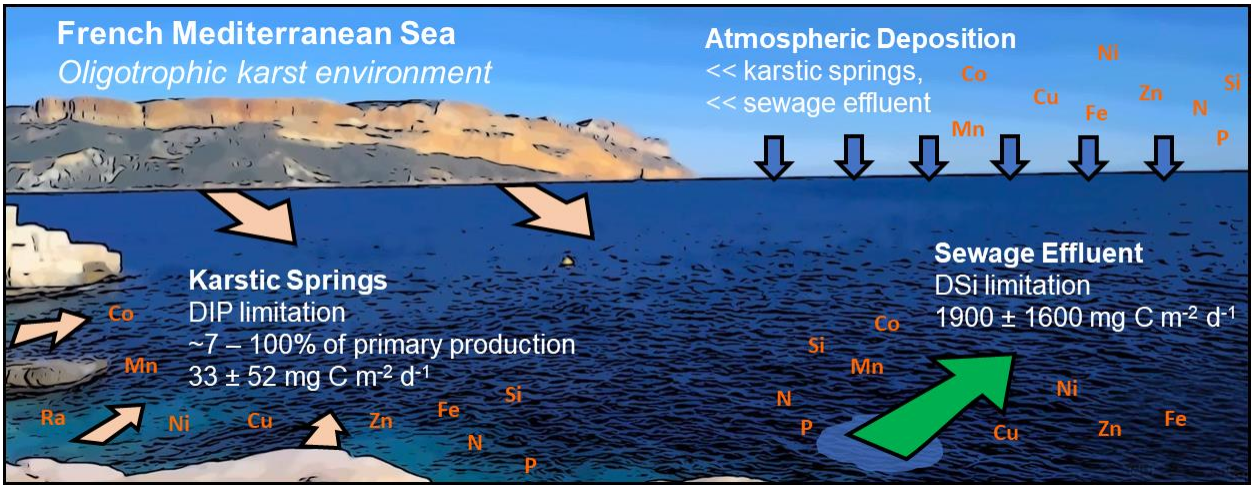

Abstract

Groundwater springs in karstified carbonate aquifers are known to transport carbon, nutrients and trace elements to the coastal ocean. The biogeochemical significance of submarine karstic springs and their impact on coastal primary production are often difficult to quantify. We investigated several karstic springs, including the first-order Port-Miou spring, in an urbanized watershed that is also severely impacted by sewage effluent (Calanques of Marseille-Cassis, France). Karstic springs were elevated in major nutrients and bioactive trace metals over Mediterranean seawater, with relatively low concentration ranges. Groundwater NO_3^- was likely derived from atmosphere-aquifer interactions, while DOC:DON ratios reveal that NO_2^- and NH_4^+ was autochthonously produced during mixing between karst groundwater and seawater. Submarine groundwater discharge (SGD) during March 2018 (wet season, baseflow conditions) was 6.7 ± 2.0 $m^3\ s^{-1}$ for the entire investigated coastline, determined from simultaneous ^{224}Ra and ^{226}Ra mass balances. The contribution of groundwater PO_4^{3-}, the major limiting nutrient of the Mediterranean Sea, sustained only 1% of primary production adjacent to sewage outfall, but between 7 and 100% of the local primary production in areas that were not impacted by sewage. Groundwater and seawater Fe:DIN and Fe:DIP ratios suggest that Fe was not a limiting micro-nutrient during the period of study, where bioactive trace metal fluxes were dominated by sewage and atmospheric deposition, although excess Fe from groundwater may locally enhance N fixation. Groundwater solute fluxes may easily vary by a factor of two or more over time because karst aquifers are sensitive to precipitation, as is the case of the regional carbonate karstified aquifer of Port-Miou, highlighting the critical importance of properly characterizing nutrient and trace metal inputs in these coastal environments.

1. Introduction

In coastal karstified carbonate aquifers, groundwater discharge often occurs as a point-source, in the form of coastal springs and submarine springs (Fleury et al., 2007a). Karstic springs carry new carbon, nutrients, trace elements, organic contaminants and even pesticides to the coastal ocean (Garcia-Solsona et al., 2010b; Gonneea et al., 2014; Montiel et al., 2018; Pavlidou et al., 2014); thus, karstic springs may play a vital role in sustaining coastal primary production (Lecher et al., 2018). The biogeochemical significance of karstic groundwater discharge in supplying nutrients and trace metals may be particularly relevant in semi-arid regions like the oligotrophic Mediterranean Sea where runoff is limited (Garcia-Solsona et al., 2010b, 2010a; Tovar-Sanchez et al., 2014; Trezzi et al., 2016) and where PO_4^{3-} broadly limits primary production (Diaz et al., 2000; Krom et al., 1991). The significance of karstic springs in sustaining or enhancing coastal zone primary production (Rodellas et al., 2014; Tovar-Sanchez et al., 2014) has received limited attention along the French Mediterranean coastline.

The Ca-carbonate matrix of karstified carbonate aquifers can remove the major nutrient PO_4^{3-} from solution via mineral precipitation (de Jonge and Villerius, 1989; Price et al., 2010); alternatively, carbonate mineral dissolution may release adsorbed P into karst groundwaters (Pain et al., 2020). The removal of P leads to groundwaters with elevated stoichiometric N:P ratios above Redfield ratio (16), which may subsequently drive the coastal ocean toward P-limitation (Conan et al., 2007; Egger et al., 2015). P mineral precipitation commonly occurs in karst aquifers of the Mediterranean Sea, with a median coastal groundwater N:P ratio of ~150 (Rodellas et al., 2015). In addition to macro-nutrients, phytoplankton also require micro-nutrients for growth. Bioactive trace metals such as Cd, Mn, Fe, Co, Ni, Cu and Zn play important roles in marine phytoplankton development (Morel and Price, 2003; Twining and Baines, 2013), since trace metals are used as cofactors (or part of cofactors) of enzymes or as structural elements in various molecules (Morel and Price, 2003). For example, Fe loading from submarine groundwater discharge (SGD) has been suggested to stimulate primary production in the South Atlantic Ocean (Windom et al., 2006). Therefore, concurrent evaluation of groundwater-borne nutrient and trace metal fluxes is required to properly understand the impacts that karstic springs may have in sustaining or enhancing coastal zone primary production.

At the basin-scale, total SGD has shown to be a significant vector in transporting major nutrients (Rodellas et al., 2015; Tamborski et al., 2018) and bioactive trace metals (Trezzi et al., 2016) to the oligotrophic Mediterranean Sea, as compared to riverine (Pujo-Pay et al., 2006) and atmospheric inputs (Herut et al., 1999). Mediterranean karst springs are significantly enriched in DIN (120 – 440 µM) and DIP (0.18 – 0.72 µM), which respectively comprise 8 – 31% and 1 – 4% of total riverine inputs to the entire Mediterranean Sea (Chen et al., 2020). At local-scales where riverine inputs are limited, karstic springs may be even more important for coastal ecosystems. For example, karst springs have been suggested to increase P-limitation along the eastern coast of Spain (Garcia-Solsona et al., 2010b) and its island coves (Garcia-Solsona et al., 2010a; Tovar-Sanchez et al., 2014). Indeed, point-sourced karstic groundwater nutrient loads can directly impact coastal biodiversity at the local-scale (Foley, 2018). However, assessment of nutrient loads from karst aquifers is difficult to accurately constrain in space and time, in part due to geologic heterogeneity and the response-time of the aquifer to precipitation (Montiel et al., 2018).

The Gulf of Lions, situated along the northwest Mediterranean Sea, hosts several known coastal and submarine springs (Bakalowicz, 2015). Bejannin et al. (2020) recently estimated karst groundwater DSi and NO_3^- fluxes along Côte Bleue, a region just west of the city of Marseille (eastern Gulf of Lions). In the absence of surface water inputs, karst groundwater is the sole nutrient source to this region and is likely responsible for sustaining coastal zone primary productivity, where karst groundwater supplies significant DSi ($6.2 \pm 5.0 * 10^3$ mol d^{-1} km^{-1}) and NO_3^- + NO_2^- ($4.0 \pm 2.0 * 10^3$ mol d^{-1} km^{-1}) offshore. Farther east, several karstic springs are known to discharge to the Calanques of Marseille-Cassis, including the springs of Sugiton, Cassis (*e.g.* the Bestouan spring) and the first-order Port-Miou spring (Arfib and Charlier, 2016; Bejannin et al., 2017; Claude et al., 2019; Fleury et al., 2007a); however, information on nutrient loads and estimates of primary productivity in this region are lacking.

Herein we provide a comprehensive analysis of the major nutrient and bioactive trace metal fluxes driven by the karstic springs of the Calanques of Marseille-Cassis during baseflow conditions (i.e. conservative) and how these karstic springs may sustain coastal zone primary production during our studied period (March 2018). This is an ideal location to study because there is little to no surface water inputs; all of the runoff during precipitation events infiltrates through the highly fractured limestone and dry paleo-valleys. In order to understand the role of the karstic springs in coastal biogeochemical cycles, calculated chemical fluxes will be compared with sewage effluent from a major urbanized Mediterranean city (Marseille) and atmospheric deposition. Thus, a major question of this research is whether or not karst groundwater is relevant in sustaining primary production in metropolitan areas impacted by sewage discharge. This study helps establish the significance of various nutrients and trace metals in the study area and aims to elucidate the possible consequences on processes such as alterations of marine ecosystem structure and function. Further, the SGD-driven chemical fluxes help to evaluate various chemical element budgets in the NW Mediterranean Sea.

2. Materials & Methods

2.1 Study Site

The Calanques of Marseille-Cassis spans a rocky, cliff-dominated shoreline of over 20 km in length along the French Mediterranean Sea (**Figure 1**). Regional precipitation is on the order of 500 – 1,000 mm a^{-1} and primarily occurs during winter, with drought-like conditions that persist during summer (Arfib and Charlier, 2016). The karst Port-Miou aquifer is composed of Jurassic and Cretaceous limestone, dolostone and mixed siliciclastic-carbonate rocks with a recharge area of over 400 km^2. The Port-Miou spring is one of the largest karstic springs in coastal Europe (Custodio, 2010) and is the primary spring of this region. The primary submarine karst spring discharges at a depth of ~12 m below sea level from a karstic conduit in excess of 100 m^2 (Fleury et al., 2007a). Karstic groundwaters are brackish, reflecting a mixture between freshwater and seawater in the upstream part of the karst network (Blavoux et al., 2004; Cavalera, 2007). A submarine dam was constructed in the 1970's in the main karst conduit to prevent further seawater intrusion; however, groundwater salinities remain elevated due to present day seawater intrusion at depth. The deep reservoir of the Port-Miou aquifer is hypothesized to have such a large mixing zone and transit time that the first-magnitude spring is considered to discharge at a relatively constant salinity (~12 – 14 PSU) and flow-rate (~ 3 m^3 s^{-1}) during baseflow conditions (i.e. no precipitation); in contrast, the shallow reservoir of the aquifer responds rapidly to precipitation and can exceed 20 m^3 s^{-1} immediately following a rainfall-event (Arfib and Charlier, 2016; Claude et al., 2019).

The Huveaune River (~0.3 – 65 m^3 s^{-1}) and Jarret River merge in the city of Marseille (**Figure 1**), where they mix with treated wastewater (~1.7 million people). The combined waters form the Cortiou sewage outfall and flows to the Mediterranean Sea (Savriama et al., 2015). The wastewater treatment plant (WWTP) can handle a maximum discharge between 3 and 6.5 m^3 s^{-1}; the remaining flow goes untreated in the event of heavy rainfall. The combined sewage and Huveaune River discharge in dry periods averages ~2.9 m^3 s^{-1} (Oursel et al., 2013). The WWTP chemical loading decreased between 1984 and 1999 with the development of a primary treatment plant (Bellan et al., 1999; Perez et al., 2005); however, eutrophication and adverse ecological phenomena persist in the region adjacent to the sewage outfall to date.

2.2 Field Methods

Seawater samples were collected offshore of the Calanques of Marseille-Cassis on 27 – 28 March 2018 aboard the *R/V Antédon II* (**Figure 1**). Surface waters were collected from ~0.5 m depth using a trace-metal-clean submersible pump. Coastal surface waters, waters from the outlet of the Cortiou WWTP and karstic springs were sampled from a Zodiac on 28 – 29 March 2018. Four submarine karstic springs were sampled by SCUBA divers, where a trace-metal-clean submersible pump was placed directly within the subterranean karst conduit. Two surficial springs were sampled in Port-Miou, which were connected to the main karst conduit (**Figure 1**). Salinity (PSU) and temperature were measured *in-situ* from the shipboard CTD sensor (conductivity/temperature/depth) and from a handheld WTW probe (Xylem) for the coastal samples aboard the Zodiac.

Continuous *in-situ* salinity time-series of the Port-Miou brackish spring were recorded with a CTD Diver sensor (15-minute time step; Schlumberger) at the underground dam, 500 m inland in the main flooded karst conduit discharging in the Calanque of Port-Miou (Port-Miou in-situ observatory). *In-situ* discharge time-series of the Huveaune River (**Figure 1**) was recorded at the State gauging station Aubagne-Huveaune (Banque Hydro #Y4424040). Rainfall was recorded in the area that encompasses the Huveaune River watershed and the recharge area of the Port-Miou and Bestouan karst springs (Arfib and Charlier, 2016) at the Aubagne State rain gauge station (Météo France #13005003; **Figure 1**).

2.3 Analytical Methods

Samples for nitrate (NO_3^-), nitrite (NO_2^-), silicate ($Si(OH)_4$) and phosphate (PO_4^{3-}) were prefiltered onto 25 mm uptidisc RC (~0.45 µm) PP, collected into 50 mL polyethylene flasks and stored frozen until analysis. Samples for ammonium (NH_4^+) determination were collected into 60 mL polycarbonate tubes and analyzed directly in the field. NO_3^-, NO_2^-, $Si(OH)_4$ and PO_4^{3-} were analyzed using an automated colorimetric method (Aminot and Kerouel, 2007). The detection limits were 0.05 µM for NO_3^-, NO_2^- and $Si(OH)_4$, and 0.02 µM for PO_4^{3-} with measurement accuracies of ± 0.02 µM, ± 0.02 µM, ± 0.005 µM and ± 0.005 µM, respectively. NH_4^+ concentration was measured by using the fluorescent procedure of Holmes et al. (1999) with a detection limit of 0.005 µM and a measurement accuracy of ± 0.015 µM. Select samples for Dissolved Organic Nitrogen (DON) and Phosphorus (DOP) were prefiltered through 2 combusted (24 h, 450°C) glass fiber filters (Whatman GF/F, 25 mm), collected in Teflon vials, then poisoned with $HgCl_2$ and stored at 4°C until analysis. In the laboratory, samples were analyzed by persulfate wet-oxidation according to Pujo-Pay and Raimbault (1994) and Pujo-Pay et al. (1997). The detection limits were 0.2 µM for DON and 0.02 µM for DOP, with measurement accuracies of ± 0.3 µM for DON and ± 0.02 µM for DOP.

Samples for Dissolved Organic Carbon (DOC) were filtered through 2 pre-combusted (24 h, 450 °C) glass fiber filters (Whatman GF/F, 25mm) and collected into a pre-combusted glass sealed ampoule acidified with orthophosphoric acid. Samples were then analyzed by high temperature catalytic oxidation (Sugimura and Suzuki, 1988) on a Shimadzu TOCL analyzer. Typical analytical precision is ±0.1–0.5 (SD) or 0.2–1% (CV). Standardization and data quality were assured through the use of consensus reference materials (http://www.rsmas.miami.edu/groups/biogeochem/CRM.html) that was injected every 12 to 17 samples to insure stable operating conditions. Particulate Organic Carbon (POC) and Nitrogen (PON) were collected on pre-combusted (24 h, 450 °C) glass fiber filters (Whatman GF/F, 25mm). Filters were dried in an oven at 50 °C and stored in ashed glass vials and in a desiccator until analysis on a CHN Perkin Elmer 2400.

For prokaryotic abundance, 1.8 mL of (select) samples were fixed with glutaraldehyde (1% final concentration). Samples were incubated for 15 minutes in the dark at ambient temperature and then stored at -80°C until flow cytometric analysis. A 1 mL sub-sample was incubated with SYBR Green I (Invitrogen−Molecular Probes) at 0.025% (v/v) final concentration for 15 minutes at room temperature in the dark. Counts were performed with a FACS Calibur flow cytometer (Becton Dickinson) equipped with an air-cooled argon laser (488 nm, 15 mW; van Wambeke et al., 2009).

Karstic spring and (select) seawater samples for trace element determination were filtered on site with disposable polypropylene syringes and Durapore membranes (0.22 µm) and stored in acid washed HDPE bottles after acidification with ultrapure HNO_3^- (1‰ v/v). Trace elements (Mn, Fe, Co, Ni, Cu and Zn) were analyzed with Q-ICPMS (iCAP Q, Thermo Scientific® equipped with an Argon Gas Dilution in-line system) after acidification at 1% v/v HNO_3^- at the AETE-ISO (Analyse des Elements en Trace dans l'Environnement et Isotopes) technical platform of the OSU OREME, University of Montpellier. The Argon Gas Dilution in-line system enables the introduction of highly mineralized samples without previous dilution. Instrument calibrations were carried out with synthetic multi-elemental solutions. Instrumental drift was monitored and corrected by addition of a multi-elemental (Be, Sc, Ge, Rh, Ir) internal standard. Reagent and procedural blanks were measured in parallel to sample treatment using identical procedures. Precision error was typically < 10%. CASS-6 seawater reference material for trace metals (National Research Council, Canada) was analyzed every 20 samples to check the analysis accuracy (**Table S1**). Mean results are within the range of certified uncertainties and deviation of measured values was < 10% of certified concentrations.

Approximately ~110 L of seawater per station was collected for Ra isotopes on board the *R/V Antédon II* (offshore samples); between ~20 and 40 L of water was collected from the coastal stations. Ra isotope samples were collected into plastic cubitainers, weighed and filtered through MnO_2-coated acrylic fibers (Mn-fiber) at a flow-rate of < 1 L min^{-1} to quantitatively adsorb dissolved Ra isotopes onto the Mn-fiber (Moore and Reid, 1973). The Mn-fibers were triple rinsed with Ra-free deionized water and partially-dried using compressed-air until a fiber-to-water ratio of 1:1 was achieved (Sun and Torgersen, 1998). The short-lived ^{223}Ra and ^{224}Ra isotopes were counted using a delayed coincidence counter (RaDeCC) (Moore and Arnold, 1996) following the counting recommendations described in Diego-Feliu et al. (2020). In the case of high activity samples, a second count was performed between 7

– 10 days after sample collection to determine the activity of ^{223}Ra. Samples were counted one month after collection to quantify ^{228}Th, in order to determine the activity of unsupported, excess ^{224}Ra (denoted $^{224}Ra_{ex}$ hereafter). Detectors were calibrated from measurements of ^{232}Th standards (Moore and Cai, 2013); activities and uncertainties were calculated following Garcia-Solsona et al. (2008). Long-lived ^{226}Ra was quantified via the ingrowth of its daughter ^{222}Rn using the RaDeCC system (Geibert et al., 2013).

2.4 Water Flow Calculations

Ra isotopes were used to quantify karstic spring inputs to the coastal zone of the Calanques of Marseille-Cassis. These isotopes are typically enriched by one to three orders of magnitude in coastal groundwaters relative to seawater, making them effective tracers of SGD in karst environments (Garcia-Solsona et al., 2010a, 2010b; Tovar-Sanchez et al., 2014). Karst aquifers are typically enriched in U relative to Th, and therefore in U-series daughters (e.g. ^{226}Ra >> ^{228}Ra; Charette et al., 2007); we thus use ^{226}Ra, in addition to ^{224}Ra, also enriched in the spring waters, in the ensuing analysis. The coastal zone of the Calanques of Marseille-Cassis was sub-divided into five unique areas, following coastal geomorphological features (boxes 1 – 5; **Figure 1**). We note that the Calanque of Port-Miou (box 4) mixes with box 5 (Cassis); in the ensuing analysis these boxes are separated from each other across the inlet of Port-Miou (**Figure 1**).

Runoff in this region is insignificant and we neglect the molecular diffusion of Ra isotopes from sediments because the coastline is predominately carbonate rock (very little unconsolidated sediment; Bejannin et al., 2017). A steady-state mass balance of short-lived ^{224}Ra ($t_{1/2}$ = 3.66 d) and long-lived ^{226}Ra ($t_{1/2}$ = 1,600 y) was constructed for each individual box,

$$\frac{d^{224}Ra}{dt} = Q^{224}_{WWTP} * {}^{224}Ra_{WWTP} + {}^{224}Ra_{SGD} * Q_{SGD} - ({}^{224}Ra_{box} * V_{box} * \lambda_{224}) - \left({}^{224}Ra_{box} - {}^{224}Ra_{sea}\right) * \frac{V_{box}}{\tau_{box}} \quad \text{(Eq. 1)}$$

$$\frac{d^{226}Ra}{dt} = Q^{226}_{WWTP} * {}^{226}Ra_{WWTP} + {}^{226}Ra_{SGD} * Q_{SGD} - \left({}^{226}Ra_{box} - {}^{226}Ra_{sea}\right) * \frac{V_{box}}{\tau_{box}} \quad \text{(Eq. 2)}$$

where Ra_{WWTP}, Ra_{SGD}, Ra_{box} and Ra_{sea} represents the mean ^{224}Ra (Eq. 1) or ^{226}Ra (Eq. 2) activity (dpm 100L^{-1}) of the wastewater treatment plant effluent, the karstic groundwater springs, the surface waters of the box under consideration and offshore Mediterranean seawater, respectively. Additional mass balance terms include the discharge of the WWTP (Q_{WWTP}; m^3 s^{-1}), submarine groundwater discharge (*i.e.* karstic spring; Q_{SGD}; m^3 s^{-1}), the volume of water within each box impacted by groundwaters (V; m^3), the ^{224}Ra decay constant (λ_{224} = 0.189 d^{-1}) and the surface water residence time of the box (τ_{box}; d). Equations 1 and 2 were simultaneously solved for each box under consideration to obtain surface water residence time and SGD flow. Note the first term on the right hand-side of each equation (Q_{WWTP}*Ra_{WWTP}) is only applicable to Cortiou (box 1; **Figure 1**). The mass balance for Cassis (box 5) includes an additional advective input term from mixing with Port-Miou (box 4; **Figure 1**), where the ^{224,226}Ra input to Cassis is equal to the ^{224,226}Ra export from Port-Miou (as calculated from Eqs. 1 & 2).

The mean ^{224}Ra and ^{226}Ra activities for each box (Ra_{box}) were calculated from a natural neighbor raster interpolation in ArcMap 10.1; minimum and maximum activities based on counting statistics were used to generate interpolation uncertainties. The volume of water impacted by SGD within each box (V) was assessed from vertical salinity profiles, determined at each station from the shipboard CTD sensor relative to Mediterranean seawater salinity. Stations T1-3, T2-4 and T9-2 (**Figure 1**) were averaged (± standard deviation) to determine the ^{224,226}Ra endmember of open seawater in the region ($^{224}Ra_{sea}$ = 1.0 ± 0.2 dpm 100L^{-1}; $^{226}Ra_{sea}$ = 15 ± 3 dpm 100L^{-1}; salinity = 37.9 ± 0.1; n = 3). Offshore seawater samples from T10 were appreciably enriched in groundwater-derived solutes and are therefore not included in the offshore seawater Ra average. Groundwater chemical element fluxes were determined for each box by multiplying the karstic spring solute concentration by the respective SGD flow for each box. The SGD flow and the chemical endmember uncertainty were propagated into the final solute flux uncertainty for each box. We assigned an apparent 50% uncertainty for surface water residence times, based on the analysis of Claude et al. (2019); box area and volumes are assigned an arbitrary uncertainty of 10%. Ra isotope endmembers for boxes 1 and 2 (where springs were not identified or sampled) are taken as the mean (± standard deviation) of the four springs sampled from boxes 4 and 5; Ra uncertainties for boxes 3 – 5 are based on analytical uncertainties (Garcia-Solsona et al., 2008). For solute endmembers (boxes 1, 2, 4 and 5), we simply use the mean (± standard deviation) of the four springs sampled from boxes 4 and 5 for each respective chemical element. Box 3 endmember concentrations are taken as the average of the two springs sampled from box 3 and uncertainties are approximately 20% for macro-nutrients and 50% for micro-nutrients given their apparent range over distinct salinities (17.8 – 26.3). Terms used in the mass balances and flux calculations are further described in **Section 3.4**.

3. Results

3.1 Hydrological and Meteorological Context

Figure 2 provides insight into the hydrological and meteorological contexts of the study. The Port-Miou brackish spring's salinity remained almost constant and high (> 13) from October 2017 up to March 01 2018, which represents a long-lasting drought period, which tends to cease in autumn for this Mediterranean climate. The Port-Miou spring salinity is highly correlated with the discharge of the regional carbonate aquifer of Port-Miou (Arfib and Charlier, 2016). Another proxy of the Port-Miou spring discharge is the Huveaune river discharge, which is supplied by runoff during rainfall events and by continental karst springs within the watershed. The Huveaune river exhibited a low discharge rate over the same period as the coastal karst spring of Port-Miou (inferred by elevated salinities). During this high salinity period (6 months), 243 mm of precipitation occurred with a low daily intensity (max 36 mm d^{-1} in Aubagne station). This precipitation recharged the soil and part of the unsaturated zone of the carbonate aquifer, but it was not sufficient to activate the high seasonal flow stage (early spring; Figure 2).

From March 01 2018, rainfall events generated small floods in the Huveaune river and karst springs, with minor contributions of the fast flow component (runoff in river or rapid karst groundwater flow, with a recession in a few days) and a low increase of baseflow lasting for a few weeks. The rainfall event two weeks before the sampling period (March 15th, 2018; 42 mm at Aubagne station and 64 mm at Plan d'Aups station; Figure 1) generated a karst flood at the Port-Miou spring (**Figure 2**), as shown by the salinity decrease over four days, followed by an increase in salinity until the next rainfall event (after the sampling period). The spring was then recovering baseflow conditions by mixing of deep flows of brackish and fresh groundwater (Arfib and Charlier, 2016). Moreover, as inferred from the very low discharge of the Huveaune River (< 1 m^3 s^{-1}) during this time period (**Figure 2**), the Cortiou sewage outfall to the sea was predominantly sourced from the WWTP and not from additional mixing with the Huveaune and Jarret rivers.

The hydrological behavior of karst aquifers in the south of France has been previously studied and successfully modeled, for instance in Fontaine de Vaucluse spring by Fleury et al., (2007b) (catchment area 1100 km²), Lez spring by Fleury et al. (2009) (catchment area 130 km²), Dardennes springs by Baudement et al. (2017) (catchment area 70 km²), and Port-Miou by Arfib and Charlier (2016) (catchment area 400 km²). All of these examples showed than more than 100 mm of cumulated rainfall is needed in autumn to begin recharging the karst aquifer. Moreover, in a Mediterranean climate, daily rainfall events are commonly higher than tens of mm, and can exceed 100 mm d^{-1} during extreme events. The period studied (2017 – 2018) was not subject to any extreme precipitation event (>100 mm d^{-1}; **Figure 2**). The rainfall event two weeks before the sampling period was thus a standard precipitation event for the season and rapid karst groundwater discharging at the springs from the shallow aquifer reservoir was thus minimal. With the preceding rainfall from September 2017 to March 2018, the aquifer recovered from drought to low-flow, representative of baseflow conditions. Therefore, we argue that the measured solute concentrations of the karstic springs are representative of baseflow conditions.

3.2 Biogeochemical Endmembers

Six different karstic springs of varying salinities (6.9 – 26.3) were sampled for chemical determinations (dissolved and particulate nutrients, trace elements and Ra isotopes) during March 2018. In general, NO_3^- (24 – 81 µM), $Si(OH)_4$ (60 – 110 µM) and PO_4^{3-} (0.15 – 0.46 µM) displayed the highest concentrations at the lowest salinities and simply followed two-endmember linear mixing between brackish groundwaters and Mediterranean seawater (**Figure 3; Table 1**). An opposite pattern was observed for NO_2^- (~0 – 0.06 µM) and NH_4^+ (0.04 – 0.23 µM; **Table 1**). Groundwater DIN:DIP ratios exhibited large variations (152 – 235; **Table 1**) but broadly fell along a dilution trend [(N:P) = -4.9582*(Salinity) + 258.75; R^2 = 0.7521; p<0.001]. Karstic groundwater concentrations did not vary greatly for DOC (40– 85 µM), POC (1.1 – 5.9 µM), DON (0.2 – 13.7 µM), PON (0.12 – 0.69 µM) and DOP (0.00 – 0.13 µM; **Table 2**). Bacterial biomass (0.99 *10^5 cell mL^{-1} for a salinity of 9.3) increased with increasing salinity to 3.6 *10^5 cell mL^{-1} for a salinity of 35 (coastal seawater). Water samples collected at the outlet of the WWTP were elevated in macro-nutrient concentrations (salinity = 21.7; **Figure 3**), reduced in DIN:DIP ratios (5; **Table 1**) and significantly enriched in bacterial biomass (**Table 2**). Elevated salinities indicate rapid mixing of sewage effluent with coastal seawater at the point of discharge.

Bioactive trace metals Mn, Fe, Co and Ni in karstic springs showed similar relationships as the dissolved nutrients, with the greatest concentrations in water samples collected adjacent to the WWTP (**Table 3**; **Figure 4**). Mn and Fe concentrations were lowest in Sugiton (7 and 17 nM; box 3) and similar between Port-Miou and Cassis (Mn 13 – 17 nM; Fe 38 – 109 nM; boxes 4 & 5). Bioactive trace metals Cu and Zn displayed mid-salinity maxima (**Figure 4**). There was a clear difference in groundwater Ra isotope activities between the three different Calanques, while water samples collected near the WWTP outlet were relatively low in dissolved Ra (**Figure 5**). Brackish groundwaters in Sugiton (box 3) were appreciably enriched in $^{224}Ra_{ex}$ (370 – 473 dpm $100L^{-1}$) despite higher salinities (**Table 4**).

3.3 Surface Waters

The salinity of coastal waters (< 4 km from shore) were lower than open Mediterranean seawaters (salinity = 38.2); the depth of waters influenced by SGD and/or sewage effluent varied from ~1 to ~5 m (**Figure 6**). Surface waters with reduced salinities were elevated in NO_3^-, PO_4^{3-}, and $Si(OH)_4$ as a consequence of terrestrial (groundwater or WWTP) inputs, with lower concentrations at higher salinities (**Figure 3**). As a result, surface waters remain elevated in NO_3^-, PO_4^{3-} and $Si(OH)_4$ (above open Mediterranean seawater concentrations) for up to several hundreds of meters beyond the point-source sewage outfall and karstic springs (boxes 4 and 5; **Figure 7**). Nutrient stoichiometric ratios indicate that surface waters and groundwaters were limited in DIP (mean DIN:DIP box 1 = 36; box 2 = 44; box 3 = 51; box 4 =141; box 5 = 73) with the exception of three surface water samples collected in the vicinity of the sewage outfall, which were limited in DSi (**Figure 8**). Bioactive trace metals Mn, Fe, Co and Ni showed similar trends as major nutrients, with higher concentrations at lower salinities, albeit with greater variability (**Figure 4**). Cu and Zn showed the greatest variability in surface waters with several samples exceeding groundwater concentrations (**Figure 4**). Ra isotopes followed two-endmember linear mixing between brackish groundwaters and Mediterranean seawater (**Figure 5**). Surface water weighted average (± standard deviation) salinity, $^{224}Ra_{ex}$ and ^{226}Ra activities for each box are summarized in **Table 5**. Surface water parameters (salinity, pH, Ra isotopes, dissolved inorganic nutrients) are summarized in **Table S2**.

3.4 SGD flows and element fluxes

Surface water residence times varied widely, from 0.6 – 39 d, depending on the selected box (**Table 5**). Submarine groundwater discharge to the entire zone of the Calanques of Marseille-Cassis is estimated as 6.7 ± 2.0 $m^3\ s^{-1}$ (5.8 ± 1.7 *10^5 $m^3\ d^{-1}$) during the study period of March 2018, and is most prevalent along the eastern section of the studied area (**Table 5**). Claude et al. (2019) estimated a surficial spring discharge equal to 0.6 ± 0.1 $m^3\ s^{-1}$ from a short-lived Ra mass balance to the Calanque of Port-Miou during baseflow conditions, compared to 1.0 ± 0.3 $m^3\ s^{-1}$ during this study (box 4; **Table 5**). Just west of Marseille, Bejannin et al. (2020) estimated SGD equal to ~0.6 $m^3\ s^{-1}$ along the karstic shoreline of Côte Bleue, or a factor of ten less than the Calanques of Marseille-Cassis. It is important to note that this SGD flow (and the chemical elements transported by SGD) is temporally variable; the shallow reservoir of the Port-Miou aquifer fluctuates in direct response to precipitation (**Figure 2**). The karstic groundwater DIN, DIP and DSi fluxes were 4.7 ± 1.6 *10^4 mol d^{-1}, 2.2 ± 0.7 *10^2 mol d^{-1} and 6.3 ± 2.0 *10^4 mol d^{-1}, respectively, over the entire study area (**Figure 9**). Approximately 70% of the SGD inputs were into Cassis (box 5); area-normalized DIN and DIP fluxes to Cassis were thus 6,700 ± 2,800 µmol N $m^{-2}\ d^{-1}$ and 29 ± 13 µmol P $m^{-2}\ d^{-1}$, respectively (DIN:DIP >230).

4. Discussion

4.1 Biogeochemical signature of the karst springs and coastal waters

The karstic springs were dominated by NO_3^-, with negligible NO_2^- and NH_4^+, indicative of a highly oxygenated aquifer system where there is little denitrification, typical of Mediterranean karst aquifers. The relatively low NO_3^- concentrations of the springs, coupled with a lack of surface water inputs, suggest that the NO_3^- is naturally derived (*i.e.* atmosphere-aquifer interactions; Garcia-Solsona et al., 2010a,b), rather than of an anthropogenic origin. In comparison, concentrations of DSi for all springs were relatively high, reflecting near-saturated equilibrium conditions with the karst aquifer matrix (*i.e.* water-rock interactions) as noted by Tamborski et al. (2018). Low groundwater DIP concentrations for all of the springs are typical of karst aquifers where DIP may co-precipitate with dissolved Ca (Slomp and van Cappellen, 2004).

The karstic spring nutrient concentrations of the Calanques of Marseille-Cassis (**Table 1**) are comparable to other karstic springs in the southern Gulf of Lions region, and more broadly to that of the entire Mediterranean Sea (excluding DIN). For example, karst springs and shallow pore water nutrient concentrations were recently investigated along Côte Bleue, a 22 km long stretch of karstic coastline just west of Marseille (Bejannin et al., 2020). Brackish springs were appreciably enriched in $Si(OH)_4$ (113 ± 40 µM) but not NO_3^- (0.02 – 4.26 µM), whereas brackish pore waters exhibited a wide range in all macro-nutrients (2 – 133 µM $Si(OH)_4$; 22 – 194 µM NO_3^- + NO_2^-; 0.01 – 4.0 µM PO_4^{3-}). Macro-nutrient concentrations of the studied springs here are comparable to the karst brackish groundwater spring (salinity ~4 – 10) of La Palme lagoon (~200 km west, western Gulf of Lions), with $Si(OH)_4$, NO_3^- and PO_4^{3-} concentrations of 114 µM, 50 – 62 µM and 0.10 – 0.43 µM, respectively (Rodellas et al., 2018; Tamborski et al., 2018). Chen et al. (2020) recently compiled karstic spring nutrient concentrations for 31 different locations along the Mediterranean Sea. Regional DIN concentrations (120 – 440 µM; salinity < 10; 1st and 3rd quartiles) are appreciably higher than the karst springs studied here over a similar salinity range, while DIP (0.18 – 0.72 µM) concentrations are comparable (**Table 1**).

There was an increase in NO_2^- and NH_4^+ concentrations along the salinity gradient (excluding sewage-impacted samples), where the karstic springs exhibited lower concentrations than Mediterranean seawater (**Figure 3**). This observation is coherent with an autochthonous production of NO_2^- and NH_4^+ during mixing, rather than a

terrestrial NO_2^- and NH_4^+ source. Indeed, bacterial biomass increased linearly along the salinity gradient (**Figure 3**). The bacterial compartment must behave as a nitrogen producer and not as a consumer. Pujo-Pay et al. (2006) showed that there is a threshold value for the DOC:DON ratio as an indicator of the trophic role of bacteria. A DOC:DON ratio below 10 indicates that bacteria meet their nitrogen needs for growth and are therefore a source of nitrogen to the ecosystem (ammonification process). Above 10, bacteria need to consume nitrogen to balance their internal needs and therefore consume DIN. The DOC:DON ratio is 0.6 for sewage effluent, 3 to 6 for Port-Miou (box 4), ~14 for Sugiton (box 3), and higher than 15 for surface and coastal waters (**Table 2**).

Karstic spring Fe concentrations (17 – 109 nM) were lower than karstic springs previously investigated in the Northwest Mediterranean (130 – 550 nM; n = 12; 1^{st} – 3^{rd} quartiles; Trezzi et al., 2016), although the springs investigated here are more saline (6.9 – 26.3 vs. 4.1 – 5.3; 1^{st} – 3^{rd} quartiles; Trezzi et al., 2016). Karstic groundwater Co and Ni concentrations were within the range of concentrations reported for the Northwest Mediterranean springs (Co = 0.14 – 0.54 nM; Ni = 2.7 – 7.9 nM), despite their higher salinity. Karstic springs for this study were higher in Cu (2 – 18 nM) and Zn (5 – 109 nM) compared to the range reported by Trezzi et al. (2016) (Cu = 2.1 – 4.6 nM; Zn = 33 – 71 nM). The karstic spring trace metal concentration ranges suggest that these bioactive metals are derived from either atmosphere-aquifer interactions or water-rock interactions, and do not reflect an anthropogenic contaminant source (Alorda-Kleinglass et al., 2019; Trezzi et al., 2016). Surface water mid-salinity maxima of Zn and Cu in Port-Miou and Cassis (boxes 4 and 5) are positive linearly correlated (excluding one outlier; $R^2 = 0.95$; $P<0.01$). Zn and Cu may be derived from antifouling paints (Charette and Buesseler, 2004; Garcia-Orellana et al., 2011) from a high density of residential boats moored in both the Calanque of Port-Miou and in Cassis harbor.

Karstic groundwater Ra isotope activities (**Table 4**, **Figure 5**) are in general agreement with previous studies for the Calanque of Port-Miou (Bejannin et al., 2017; Claude et al., 2019). The relatively lower ^{226}Ra activities of the Bestouan submarine spring (box 5; 318 – 324 dpm $100L^{-1}$), as compared to the Port-Miou spring (box 4; 506 – 525 dpm $100L^{-1}$, box 4; **Table 4**) is a function of the salinity of the groundwater and its origin (Romey et al., 2014). Although both the Bestouan and Port-Miou springs share a common recharge area, the brackish groundwater of the Bestouan spring originates from a freshwater surface stream 2 km inland from the sea that infiltrates into the karst, where it mixes with a deeper reservoir and thus decreases the salinity of the deep brackish groundwater. Therefore, the ^{226}Ra activity of the Port-Miou spring is likely higher because it is only a mixture between deep circulated seawater and fresh groundwater, whereas the Bestouan spring is mixed with a third surficial component with relatively low ^{226}Ra activity.

4.2 Chemical fluxes from SGD, WWTP and atmospheric deposition

To determine the relative significance of macro and micro-nutrient fluxes associated with submarine karstic springs to the Calanques of Marseille-Cassis, we compared the magnitude of groundwater nutrient loads to that of the WWTP of Cortiou and from atmospheric deposition. Previous studies estimated dissolved and particulate solute fluxes from the Cortiou sewage outfall during the dry season (~250,000 $m^3\ d^{-1}$; Oursel et al., 2014, 2013). Dust deposition, particularly from the Sahara Desert, may represent a potentially significant source of chemical elements to the Mediterranean Sea and fluxes are likely more significant under intense rainfall (Durrieu de Madron et al., 2011; Garcia-Orellana et al., 2006). Nutrient and trace metal total (wet and dry) atmospheric depositional fluxes were compiled from the literature for nearby regions (**Table S3**). Atmospheric deposition fluxes were calculated considering a coastal surface area of 23.1 km^2 (boxes 1 – 5; **Figure 1**). It is important to note that we assume that the atmospheric deposition fluxes are representative of the total (wet and dry) depositional processes occurring in the coastal zone of the Calanques of Marseille-Cassis during the study period; atmospheric and WWTP fluxes serve only as first-order approximations.

Macro- and micro-nutrient fluxes from SGD, WWTP and atmospheric deposition to the Calanques of Marseille-Cassis are summarized in **Figure 9**. The karstic groundwater solute fluxes calculated in this study are a snapshot view that we consider near representative of baseflow conditions for the Calanques of Marseille-Cassis (**Figure 2**). In general, WWTP macro- and micro-nutrient loads exceeded inputs from karstic groundwaters during the studied period, except for DSi. In contrast, groundwater solute fluxes generally exceeded inputs from total atmospheric deposition, aside from dissolved Fe (**Figure 9 a,b**). Macro-nutrient groundwater loads to Cassis (box 5) are normalized to the shoreline length of the considered box (6 km), resulting in $Si(OH)_4$ and NO_3^- fluxes of 11 ± 3 $*10^3$ mol d^{-1} km^{-1} and 8 ± 3 $*10^3$ mol d^{-1} km^{-1}, respectively. These karst groundwater baseflow nutrient fluxes are comparable to karst groundwater $Si(OH)_4$ (6.2 ± 5.0 $*10^3$ mol d^{-1} km^{-1}) and $NO_3^- + NO_2^-$ (4.0 ± 2.0 $*10^3$ mol d^{-1} km^{-1}) loads to Côte Bleue (just west of Marseille), assessed over multiple seasons (Bejannin et al., 2020), and are similar to flux estimates from a sandy alluvial shoreline farther west along the Gulf of Lions (2.4 ± 1.4 $*10^3$ mol Si d^{-1} km^{-1} and 5.7 ± 3.2 $*10^3$ mol N d^{-1} km^{-1}; Tamborski et al., 2018). Interestingly, Bejannin et al. (2020) note that these point-

source karstic spring macro-nutrient fluxes are comparable to fluxes along the sandy alluvial shoreline of La Palme to the west, within the Gulf of Lions, where nutrient loads are thought to be driven by a combination of subsurface lagoon-seawater exchange and seawater circulation through permeable coastal sediments (Tamborski et al., 2019, 2018).

Sewage inputs occur along the western region of the Calanques (box 1; **Figure 1**) while karstic groundwaters more broadly impact the entire coastal zone (**Figure 7**), and are greatest along the eastern region, particularly from the springs of Port-Miou and Cassis (boxes 4 & 5; **Table 5**). The significance of atmospheric deposition, as compared to SGD and riverine inputs, is proportional to the area under consideration; the larger offshore area considered, the more significant atmospheric trace metal deposition becomes (Trezzi et al., 2016). For the entire Mediterranean Sea, DIN and DSi inputs from SGD are estimated to be significantly greater than atmospheric deposition, while DIP inputs are similar (Rodellas et al., 2015). For the Calanques of Marseille-Cassis, atmospheric deposition is negligible over a spatial scale of meters to hundreds of meters away from the karstic springs, where groundwater (or sewage) is the dominant vector of solute transport to the coastal ocean (e.g. **Figure 7**). The area-normalized DIN (6,700 ± 2,800 μmol N m^{-2} d^{-1}) and DIP (29 ± 13 μmol P m^{-2} d^{-1}) fluxes to Cassis (box 5) are one order of magnitude greater than atmospheric deposition (**Table S3**).

4.3 Significance of Chemical Fluxes

4.3.1 Major Nutrient Fluxes

The Mediterranean Sea is primarily limited in phosphorous (Krom et al., 1991; Pujo-Pay et al., 2011); therefore, any DIP input from karstic springs or sewage to the coastal sea should be considered potentially significant, as it may change the geochemical conditions of the water column (**Figure 8**). DIP mixing plots for Port-Miou and Cassis indicate significant DIP concentrations in brackish surface waters during the studied period (**Figure 3**); therefore, the impact of SGD in supplying DIP (and other solutes) occurs over a scale of several kilometers (from at least 6 individual springs), despite being point-sources (**Figure 7**). As a first-order approximation, we can evaluate how much DIP is removed by primary production from a coastal DIP budget (Kim et al., 2011; Luo et al., 2014) considering equation (3),

$$P_{SGD} + P_{WWTP} + P_{atm} - P_{mix} = P_{uptake} \quad \text{(Eq. 3)}$$

where P_{SGD}, P_{WWTP}, P_{atm}, P_{mix} and P_{uptake} are the DIP fluxes (mol d^{-1}) to each respective box from SGD, the WWTP, total atmospheric deposition, mixing losses with offshore seawater and uptake from biological production, respectively. DIP inputs from SGD, the WWTP and total atmospheric deposition have been previously evaluated (Sections 3.4 & 4.2; **Figure 9**). The loss of DIP from mixing with offshore Mediterranean seawater is evaluated similarly to the mixing loss of Ra (Eqs. 1 & 2), taken as the concentration difference between the mean DIP concentration in each coastal box and offshore Mediterranean seawater (0.025 μM), with respect to the volume of water impacted by groundwater and the surface water residence time (**Table 5**).

During baseflow conditions, SGD is relatively insignificant in the DIP budget of the western Calanques and becomes increasingly more important in the eastern Calanques; the relative percent contribution of each DIP source and sink is shown in **Figure 10**. In Sugiton (box 3), DIP is rapidly removed within the first 10 m of the karstic springs (**Figure 7**), with groundwater sustaining 7 (±1) % of the DIP uptake. Mixing losses approximately balance groundwater DIP inputs to Port-Miou (i.e. no biological consumption; box 4), unsurprising given the relatively short surface water residence time (0.6 ± 0.3 d; **Table 5**) and the observed conservative behavior of DIP, with respect to groundwater-seawater mixing (**Figure 3**, **Figure 7**). Importantly, this suggests that groundwater-derived DIP may persist in the coastal ocean for at least a half day before it is significantly impacted by primary producers. In comparison, SGD accounts for more than 100% of the DIP uptake in Cassis (box 5) where surface water residence times exceed 2 days (**Table 5**), with a net consumption of 140 ± 220 mol P d^{-1} (**Figure 10**). The large uncertainty is derived from the additional mixing term between Port-Miou and Cassis (boxes 4 and 5), and between Cassis and the open Mediterranean Sea.

The groundwater DIP flux to the 20 km shoreline of the Calanques of Marseille-Cassis accounts for only 2.7 (±1.0) % of the total DIP uptake (8.3 ± 6.9 *10^3 mol d^{-1}) during baseflow conditions, unsurprising as the sewage DIP flux is two orders of magnitude greater than SGD (**Figure 9**). Assuming a Redfield Ratio of 106:16:1.0 (C:N:P) for phytoplankton (Pujo-Pay et al., 2011) and assuming that all of the DIP supplied is utilized by biological production, then primary production supported by sewage DIP loading equals 1,900 ± 1,600 mg C m^{-2} d^{-1} over the surface area of Cortiou (box 1). However, three surface water samples collected near the sewage outfall were limited in DSi (**Figure 8**), suggesting the above primary production estimate may be too high. DSi limitation in Cortiou is ultimately driven by the extreme DIN and DIP sewage loads (**Figures 3 & 9**).

Considering the surface area of Cassis (box 5), the primary production associated with DIP consumption is 33 ± 52 mg C m^{-2} d^{-1}, or ~1% of the total production stimulated by sewage effluent DIP loading to Cortiou (box 1). This rate of primary production is similar to other coastal environments impacted by SGD, as summarized by Wang et al. (2018). Thus, while the groundwater DIP flux to the Calanque of Cassis is small compared to the WWTP, it is nonetheless significant at a local and regional-scale in supporting primary production during baseflow conditions (**Figures 9 & 10**). Similarly, the groundwater DIN (3.6 ± 1.5 *10^4 mol d^{-1}) and DSi (4.7 ± 2.0 *10^4 mol d^{-1}) loads to Cassis (box 5) may help sustain biological production, as there are no other major nutrient sources in this region. SGD may further facilitate primary production in the days immediately following a rainfall event (**Figure 2**), assuming that the karstic spring nutrient concentrations are not significantly diluted. Note that certain algal species may be physically impacted by the presence of karstic springs, irrespective of nutrient loading, through environmental gradients in pH, oxygen or salinity (Foley, 2018; Lecher et al., 2018). For example, Cohu et al. (2013) concluded that reduced salinity from the Bestouan karstic spring retarded the development of the harmful algae *Ostreopsis* cf. *ovata* in Cassis because the dinoflagellate is more adapted to marine environmental conditions, despite excess NO_3^- and $Si(OH)_4$ inputs from groundwaters. Thus, SGD may also negatively impact certain phytoplankton and bacteria species development by altering local environmental gradients (e.g. **Figure 3**); this topic requires further study.

4.3.2 Micro Nutrient Fluxes

Groundwater Mn and Fe fluxes are one order of magnitude lower than sewage fluxes during baseflow conditions (**Figure 9**). Groundwater Fe may be derived from aquifer mineral weathering or atmosphere-aquifer interactions. Fe is typically added as a flocculant during wastewater treatment, which likely explains the high concentrations observed near the sewage outlet (**Figure 4**). Similar to DIP, the SGD-driven Fe flux (48 ± 21 mol d^{-1}) primarily occurs along the eastern region of the Calanques, whereas sewage inputs dominate farther west (640 ± 180 mol d^{-1}) with considerable inputs from atmospheric deposition (230 ± 160 mol d^{-1}) over the entire coastal area (**Figure 9**). It remains to be seen what proportion of Fe supplied by atmospheric deposition is bioavailable. Atmospheric Fe loads to the Mediterranean Sea are seasonally variable, and surface water Fe concentrations are typically lowest during spring blooms (Bonnet and Guieu, 2006). Increased Fe loading from SGD during the spring may play an important role in regulating primary production, particularly after a heavy rainfall event (i.e. **Figure 2**). The karstic springs investigated here have Fe:P ratios between 0.11 and 0.24, and Fe:N ratios between 710 and 2140. Such ratios demonstrate an abundance of Fe; indeed, coastal seawater Fe:P (0.12 – 0.80) and Fe:N (2 – 800) ratios suggests that Fe was not limiting primary production during the studied baseflow period. However, relatively high Fe may locally enhance nitrogen fixation (Bonnet and Guieu, 2006). The SGD area-normalized Fe flux is 7 ± 4 µmol m^{-2} d^{-1} to Cassis (box 5), within the range reported by Trezzi et al. (2016) to the NW Mediterranean Sea.

Sewage inputs of Co, Ni and Cu were approximately one order of magnitude greater than SGD, while Zn inputs were similar (**Figure 9**). Oursel et al. (2014) analyzed particles adjacent to the Cortiou sewage outlet (box 1) and found that Cu, Ni and Zn were anthropogenically derived from non-treated sewage. Sewage effluent has fundamentally altered the structure of local benthic communities in the vicinity of the Cortiou sewage outfall (Bellan et al., 1999). It is unlikely that SGD plays a major role in supplying these trace elements to the western Calanques; however, trace metal fluxes may be significant in the eastern Calanques adjacent to the Port-Miou and Bestouan springs (**Figures 4 & 9**).

Antifouling boat paint is a potential source of Cu and Zn (Charette and Buesseler, 2004; Garcia-Orellana et al., 2011), as the Calanque of Port-Miou and Cassis both host several dozen boats. We can simply compare the Cu and Zn inventory supplied by SGD (SGD element flux * surface water residence time) to the total element inventory observed in the Calanque of Port-Miou (box 4). The total inventory is calculated as the excess metal concentration (mean concentration minus Mediterranean seawater; n = 6) multiplied by the volume of water impacted by groundwater; note that this simple calculation does not account for the complex biogeochemical cycling of these metals (Rodellas et al., 2014). For the Calanque of Port-Miou, SGD supplies 1 (± 1) % of the Cu inventory and 11 (± 12) % of the Zn inventory. Thus, SGD is relatively minor in the transfer of these bioactive metals to the coastal Mediterranean Sea here.

5. Summary & Conclusions

Coastal-zone primary production can be sustained by the allochthonous nutrient and bioactive trace metal fluxes from karstic springs, particularly in oligotrophic environments like the Mediterranean Sea. For the Calanques of Marseille-Cassis, groundwater discharge is highly variable in time, as inferred from *in-situ* salinity measurements of the first-order Port-Miou spring. It remains to be seen how element fluxes may impact primary production at different times of the year, for example after a strong precipitation event or during the summer when the water column is stratified due to the permanent presence of a thermocline. Under wet season baseflow conditions (March 2018), major nutrient and bioactive trace metal inputs were dominated by sewage effluent, aside from DSi, with

minor contributions from atmospheric deposition. However, outside of the influence of sewage effluent, groundwater became the dominant nutrient vector and supported between 7 and ~100% of the estimated primary production, depending upon the Calanque. At a local-scale, karstic groundwater springs reduce P-limitation and supply excess Fe, which may locally enhance nitrogen fixation. The karstic springs studied here also broadly serve to provide new chemical elements to the Mediterranean Sea, thereby impacting the various element (and potentially isotopic) budgets.

6. Acknowledgements

This study was funded by the MED-SGD project funded by ANR (ANR-15-CE01-0004; PI: Pieter van Beek). The postdoctoral fellowship of Joseph Tamborski is supported by FEDER funded by Europe and Région Occitanie Pyrénées-Méditerranée (SELECT project; PIs: Pieter van Beek and Marc Souhaut). Jordi Garcia Orellana wants to thank the support of the Generalitat de Catalunya to MERS (2018 SGR-1588). This work is contributing to the ICTA 'Unit of Excellence' (MinECo, MDM2015-0552). This work benefited from the Port-Miou in-situ observatory within the framework of the KARST observatory network (www.sokarst.org) initiative from the INSU/CNRS. Rainfall data are provided by Météo-France. We thank the captain and crew of RV Antédon II for help during sampling at sea, including Simon Bejannin and Emilie Le Roy at LEGOS. We thank Dorian Guillemain, Nagib Bhairy, Deny Malengros and Christian Grenz at MIO for providing the CTD data. We thank Remi Freydier at AETE-ISO Platform, OSU-OREME/Université de Montpellier, for performing trace element analyses and Olivier Crispi at LOMIC, Banyuls-sur-Mer.

7. Appendix A. Supplementary data

Supplementary data to this article can be found online at https://doi.org/10.1016/j.scitotenv.2020.139106.

8. References

Alorda-Kleinglass, A., Garcia-Orellana, J., Rodellas, V., Cerdà-Domènech, M., Tovar-Sánchez, A., Diego-Feliu, M., Trezzi, G., Sánchez-Quilez, D., Sanchez-Vidal, A., Canals, M., 2019. Remobilization of dissolved metals from a coastal mine tailing deposit driven by groundwater discharge and porewater exchange. Science of the Total Environment 688, 1359–1372. https://doi.org/10.1016/j.scitotenv.2019.06.224

Aminot, A., Kerouel, R., 2007. Dosage automatique des nutriments dans les eaux marines: méthodes en flux continu. Ed. Ifremer, Méthodes d'analyse en milieu marin, 188 pp.

Arfib, B., Charlier, J.-B., 2016. Insights into saline intrusion and freshwater resources in coastal karstic aquifers using a lumped Rainfall-Discharge-Salinity model (the Port-Miou brackish spring, SE France). Journal of Hydrology 540, 148–161. https://doi.org/0.1016/j.jhydrol.2016.06.010

Bakalowicz, M., 2015. Karst and karst groundwater resources in the Mediterranean. Environmental Earth Sciences 74, 5–14. https://doi.org/10.1007/s12665-015-4239-4

Baudement, C., Arfib, B., Mazzilli, N., Jouves, J., Lamarque, T., Guglielmi, Y., 2017. Groundwater management of a highly dynamic karst by assessing baseflow and quickflow with a rainfall-discharge model (Dardennes springs, SE France) 188, 40. https://doi.org/10.1051/bsgf/2017203

Bejannin, S., Tamborski, J.J., van Beek, P., Souhaut, M., Stieglitz, T., Radakovitch, O., Claude, C., Conan, P., Pujo-Pay, M., Crispi, O., le Roy, E., Estournel, C., 2020. Nutrient Fluxes Associated With Submarine Groundwater Discharge From Karstic Coastal Aquifers (Côte Bleue, French Mediterranean Coastline). Frontiers in Environmental Science 7. https://doi.org/10.3389/fenvs.2019.00205

Bejannin, S., van Beek, P., Stieglitz, T., Souhaut, M., Tamborski, J., 2017. Combining airborne thermal infrared images and radium isotopes to study submarine groundwater discharge along the French Mediterranean coastline. Journal of Hydrology: Regional Studies 13. https://doi.org/10.1016/j.ejrh.2017.08.001

Bellan, G., Bourcier, M., Salen-Picard, C., Arnoux, A., Casserley, S., 1999. Benthic ecosystem changes associated with wastewater treatment at Marseille: Implications for the protection and restoration of the Mediterranean coastal shelf ecosystems. Water Environment Federation 71, 483–493.

Blavoux, B., Gilli, E., Rousset, C., 2004. Alimentation et origine de la salinité de la source sous-marine de Port-Miou (Marseille–Cassis). Principale émergence d'un réseau karstique hérité du Messinien. C.R. Geoscience 336, 523–533. https://doi.org/10.1016/j.crte.2003.10.027

Bonnet, S., Guieu, C., 2006. Atmospheric forcing on the annual iron cycle in the western Mediterranean Sea: A 1-year survey. Journal of Geophysical Research 111, C09010. https://doi.org/10.1029/2005JC003213

Cavalera, T., 2007. Etude du fonctionnement et du bassin d'alimentation de la source sous-marine de Port Miou (Cassis, Bouches-du-Rhone). Approche multicritere. Université de Provence - Aix-Marseille.

Charette, M. a, Moore, W.S., Burnett, W.C., 2007. CHAPTER-5 Uranium-and Thorium- Series Nuclides as Tracers of Submarine Groundwater Discharge CHAPTER-5 Uranium-and Thorium-Series Nuclides as Tracers of Submarine Groundwater Discharge. Radioactivity in the Environment 13, 234–289. https://doi.org/10.1016/S1569-4860(07)00005-8

Charette, M.A., Buesseler, K.O., 2004. Submarine groundwater discharge of nutrients and copper to an urban subestuary of Chesapeake Bay (Elizabeth River). Limnology and Oceanography 49, 376–385. https://doi.org/10.4319/lo.2004.49.2.0376

Chen, X., Cukrov, Neven, Santos, I.R., Rodellas, V., Cukrov, Nuša, Du, J., 2020. Karstic submarine groundwater discharge into the Mediterranean: Radon-based nutrient fluxes in an anchialine cave and a basin-wide upscaling. Geochimica et Cosmochimica Acta 268, 467–484. https://doi.org/10.1016/J.GCA.2019.08.019

Claude, C., Cockenpot, S., Arfib, B., Meulé, S., Radakovitch, O., 2019. Accuracy and sensitivity of radium mass balances in assessing karstic submarine groundwater discharge in the stratified Calanque of Port-Miou (Mediterranean Sea). Journal of Hydrology 578, 124034. https://doi.org/10.1016/J.JHYDROL.2019.124034

Cohu, S., Mangialajo, L., Thibaut, T., Blanfuné, A., Marro, S., Lemé, R., 2013. Proliferation of the toxic dinoflagellate Ostreopsis cf. ovata in relation to depth, biotic substrate and environmental factors in the North West Mediterranean Sea. https://doi.org/10.1016/j.hal.2013.01.002

Conan, P., Søndergaard, M., Kragh, T., Thingstad, F., Pujo-Pay, M., Williams, P.J. le B., Markager, S., Cauwet, G., Borch, N.H., Evans, D., Riemann, B., 2007. Partitioning of organic production in marine plankton communities: The effects of inorganic nutrient ratios and community composition on new dissolved organic matter. Limnology and Oceanography 52, 753–765. https://doi.org/10.4319/lo.2007.52.2.0753

Custodio, E., 2010. Coastal aquifers of Europe: an overview. Hydrogeology Journal 18, 269–280. https://doi.org/10.1007/s10040-009-0496-1

de Jonge, V.N., Villerius, L.A., 1989. Possible role of carbonate dissolution in estuarine phosphate dynamics. Limnology and Oceanography 34, 332–340. https://doi.org/10.4319/lo.1989.34.2.0332

Diaz, F., Raimbault, P., Conan, P., 2000. Small-scale study of primary productivity during spring in a Mediterranean coastal area (Gulf of Lions). Continental Shelf Research 20, 975–996. https://doi.org/10.1016/S0278-4343(00)00006-6

Diego-Feliu, M., Rodellas, V., Alorda-Kleinglass, A., Tamborski, J., van Beek, P., Heins, L., Bruach J.M., Arnold, R., Garcia-Orellana, J., 2020. Guidelines and limits for the quantification of U/Th series radionuclides with the radium delayed coincidence counter (RaDeCC). Journal of Geophysical Research: Oceans 125. https://doi.org/https://doi.org/10.1029/2019JC015544

Durrieu de Madron, X., Guieu, C., Sempéré, R., Conan, P., Cossa, D., D'Ortenzio, F., Estournel, C., Gazeau, F., Rabouille, C., Stemmann, L., Bonnet, S., Diaz, F., Koubbi, P., Radakovitch, O., Babin, M., Baklouti, M., Bancon-Montigny, C., Belviso, S., Bensoussan, N., Bonsang, B., Bouloubassi, I., Brunet, C., Cadiou, J.F., Carlotti, F., Chami, M., Charmasson, S., Charrière, B., Dachs, J., Doxaran, D., Dutay, J.C., Elbaz-Poulichet, F., Eléaume, M., Eyrolles, F., Fernandez, C., Fowler, S., Francour, P., Gaertner, J.C., Galzin, R., Gasparini, S., Ghiglione, J.F., Gonzalez, J.L., Goyet, C., Guidi, L., Guizien, K., Heimbürger, L.E., Jacquet, S.H.M., Jeffrey, W.H., Joux, F., le Hir, P., Leblanc, K., Lefèvre, D., Lejeusne, C., Lemé, R., Loÿe-Pilot, M.D., Mallet, M., Méjanelle, L., Mélin, F., Mellon, C., Mérigot, B., Merle, P.L., Migon, C., Miller, W.L., Mortier, L., Mostajir, B., Mousseau, L., Moutin, T., Para, J., Pérez, T., Petrenko, A., Poggiale, J.C., Prieur, L., Pujo-Pay, M., Pulido-Villena, Raimbault, P., Rees, A.P., Ridame, C., Rontani, J.F., Ruiz Pino, D., Sicre, M.A., Taillandier, V., Tamburini, C., Tanaka, T., Taupier-Letage, I., Tedetti, M., Testor, P., Thébault, H., Thouvenin, B., Touratier, F., Tronczynski, J., Ulses, C., van Wambeke, F., Vantrepotte, V., Vaz, S., Verney, R., 2011. Marine

ecosystems' responses to climatic and anthropogenic forcings in the Mediterranean. Progress in Oceanography. https://doi.org/10.1016/j.pocean.2011.02.003

Egger, M., Jilbert, T., Behrends, T., Rivard, C., Slomp, C.P., 2015. Vivianite is a major sink for phosphorous in methanogenic coastal surface sediments. Geochmica et Cosmochimica Acta. https://doi.org/http://dx.doi.org/10.1016/j.gca.2015.09.012

Fleury, P., Bakalowicz, M., de Marsily, G., 2007a. Submarine springs and coastal karst aquifers: A review. Journal of Hydrology 339, 79–92. https://doi.org/10.1016/J.JHYDROL.2007.03.009

Fleury, P., Ladouche, B., Conroux, Y., Jourde, H., Dörfliger, N., 2009. Modelling the hydrologic functions of a karst aquifer under active water management – The Lez spring. Journal of Hydrology 365, 235–243. https://doi.org/10.1016/J.JHYDROL.2008.11.037

Fleury, P., Plagnes, V., Bakalowicz, M., 2007b. Modelling of the functioning of karst aquifers with a reservoir model: Application to Fontaine de Vaucluse (South of France). Journal of Hydrology 345, 38–49. https://doi.org/10.1016/J.JHYDROL.2007.07.014

Foley, L., 2018. Karst-channelled intertidal submarine groundwater discharge (SGD) conditions the form of the rock pool sessile assemblage. Estuarine, Coastal and Shelf Science. https://doi.org/10.1016/J.ECSS.2018.08.014

Garcia-Orellana, J., Cañas, L., Masqué, P., Obrador, B., Olid, C., Pretus, J., 2011. Chronological reconstruction of metal contamination in the Port of Maó (Minorca, Spain). Marine Pollution Bulletin 62, 1632–1640. https://doi.org/10.1016/J.MARPOLBUL.2011.06.013

Garcia-Orellana, J., Sanchez-Cabeza, J.A., Masqué, P., Àvila, A., Costa, E., Loÿe-Pilot, M.D., Bruach-Menchén, J.M., 2006. Atmospheric fluxes of ^{210}Pb to the western Mediterranean Sea and the Saharan dust influence. Journal of Geophysical Research 111, D15305. https://doi.org/10.1029/2005JD006660

Garcia-Solsona, E., Garcia-Orellana, J., Masque, P., Dulaiova, H., 2008. Uncertainties associated with Ra-223 and Ra-224 measurements in water via a Delayed Coincidence Counter (RaDeCC). Marine Chemistry 109, 198–219. https://doi.org/10.1016/j.marchem.2007.11.006

Garcia-Solsona, E., Garcia-Orellana, J., Masque, P., Garces, E., Radakovitch, O., Mayer, A., Estrade, S., Basterretxea, G., 2010a. An assessment of karstic submarine groundwater and associated nutrient discharge to a Mediterranean coastal area (Balearic Islands, Spain) using radium isotopes. Biogeochemistry 97, 211–229. https://doi.org/10.1007/s10533-009-9368-y

Garcia-Solsona, E., Garcia-Orellana, J., Masque, P., Rodellas, V., Mejias, M., Ballesteros, B., Dominguez, J.A., 2010b. Groundwater and nutrient discharge through karstic coastal springs (Castello, Spain). Biogeosciences 7, 2625–2638. https://doi.org/10.5194/bg-7-2625-2010

Geibert, W., Rodellas, V., Annett, A., van Beek, P., Garcia-Orellana, J., Hsieh, Y.-T., Masque, P., 2013. ^{226}Ra determination via the rate of ^{222}Rn ingrowth with the Radium Delayed Coincidence Counter (RaDeCC). Limnology and Oceanography: Methods 11, 594–603. https://doi.org/10.4319/lom.2013.11.594

Gonneea, M.E., Charette, M.A., Liu, Q., Herrera-Silveira, J.A., Morales-Ojeda, S.M., 2014. Trace element geochemistry of groundwater in a karst subterranean estuary (Yucatan Peninsula, Mexico). Geochimica et Cosmochimica Acta 132, 31–49. https://doi.org/http://dx.doi.org/10.1016/j.gca.2014.01.037

Guieu, C., Loÿe-Pilot, M.D., Benyahya, L., Dufour, A., 2010. Spatial variability of atmospheric fluxes of metals (Al, Fe, Cd, Zn and Pb) and phosphorus over the whole Mediterranean from a one-year monitoring experiment: Biogeochemical implications. Marine Chemistry 120, 164–178. https://doi.org/10.1016/j.marchem.2009.02.004

Herut, B., Krom, M.D., Pan, G., Mortimer, R., 1999. Atmospheric input of nitrogen and phosphorus to the Southeast Mediterranean: Sources, fluxes, and possible impact. Limnology and Oceanography 44, 1683–1692. https://doi.org/10.4319/lo.1999.44.7.1683

Holmes, R.M., Aminot, A., Kérouel, R., Hooker, B.A., Peterson, B.J., 1999. A simple and precise method for measuring ammonium in marine and freshwater ecosystems. Canadian Journal of Fisheries and Aquatic Sciences 56, 1801–1808. https://doi.org/10.1139/f99-128

Kim, G., Kim, J.S., Hwang, D.W., 2011. Submarine groundwater discharge from oceanic islands standing in oligotrophic oceans: Implications for global biological production and organic carbon fluxes. Limnology and Oceanography 56, 673–682. https://doi.org/10.4319/lo.2011.56.2.0673

Krom, M.D., Kress, N., Brenner, S., Gordon, L.I., 1991. Phosphorus limitation of primary productivity in the eastern Mediterranean Sea. Limnology and Oceanography 36, 424–432. https://doi.org/10.4319/lo.1991.36.3.0424

Lecher, A., Mackey, K., Lecher, A.L., Mackey, K.R.M., 2018. Synthesizing the Effects of Submarine Groundwater Discharge on Marine Biota. Hydrology 5, 60. https://doi.org/10.3390/hydrology5040060

Luo, X., Jiao, J.J., Moore, W.S., Lee, C.M., 2014. Submarine groundwater discharge estimation in an urbanized embayment in Hong Kong via short-lived radium isotopes and its implication of nutrient loadings and primary production. Marine Pollution Bulletin 82, 144–154. https://doi.org/10.1016/J.MARPOLBUL.2014.03.005

Montiel, D., Dimova, N., Andreo, B., Prieto, J., García-Orellana, J., Rodellas, V., 2018. Assessing submarine groundwater discharge (SGD) and nitrate fluxes in highly heterogeneous coastal karst aquifers: Challenges and solutions. Journal of Hydrology 557, 222–242. https://doi.org/10.1016/J.JHYDROL.2017.12.036

Moore, W.S., Arnold, R., 1996. Measurement of Ra-223 and Ra-224 in coastal waters using a delayed coincidence counter. Journal of Geophysical Research-Oceans 101, 1321–1329. https://doi.org/10.1029/95JC03139

Moore, W.S., Cai, P., 2013. Calibration of RaDeCC systems for 223Ra measurements. Marine Chemistry 156, 130–137. https://doi.org/10.1016/j.marchem.2013.03.002

Moore, W.S., Reid, D.F., 1973. Extraction of radium from natural waters using manganese-impregnated acrylic fibers. Journal of Geophysical Research 78, 8880–8886. https://doi.org/10.1029/JC078i036p08880

Morel, F.M.M., Price, N.M., 2003. The biogeochemical cycles of trace metals in the oceans. Science (New York, N.Y.) 300, 944–7. https://doi.org/10.1126/science.1083545

Oursel, B., Garnier, C., Durrieu, G., Mounier, S., Omanović, D., Lucas, Y., 2013. Dynamics and fates of trace metals chronically input in a Mediterranean coastal zone impacted by a large urban area. Marine Pollution Bulletin 69, 137–149. https://doi.org/10.1016/J.MARPOLBUL.2013.01.023

Oursel, B., Garnier, C., Pairaud, I., Omanović, D., Durrieu, G., Syakti, A.D., le Poupon, C., Thouvenin, B., Lucas, Y., 2014. Behaviour and fate of urban particles in coastal waters: Settling rate, size distribution and metals contamination characterization. Estuarine, Coastal and Shelf Science 138, 14–26. https://doi.org/10.1016/J.ECSS.2013.12.002

Pain, A.J., Martin, J.B., Young, C.R., Valle-Levinson, A., Mariño-Tapia, I., 2020. Carbon and phosphorus processing in a carbonate karst aquifer and delivery to the coastal ocean. Geochimica et Cosmochimica Acta 269, 484–495. https://doi.org/10.1016/J.GCA.2019.10.040

Pavlidou, A., Papadopoulos, V.P., Hatzianestis, I., Simboura, N., Patiris, D., Tsabaris, C., 2014. Chemical inputs from a karstic submarine groundwater discharge (SGD) into an oligotrophic Mediterranean coastal area. Science of The Total Environment 488–489, 1–13. https://doi.org/10.1016/J.SCITOTENV.2014.04.056

Perez, T., Longet, D., Schembri, T., Rebouillon, P., Vacelet, J., 2005. Effects of 12 years' operation of a sewage treatment plant on trace metal occurrence within a Mediterranean commercial sponge (Spongia officinalis, Demospongiae). Marine Pollution Bulletin 50, 301–309. https://doi.org/10.1016/J.MARPOLBUL.2004.11.001

Price, R.M., Savabi, M.R., Jolicoeur, J.L., Roy, S., 2010. Adsorption and desorption of phosphate on limestone in experiments simulating seawater intrusion. Applied Geochemistry 25, 1085–1091. https://doi.org/10.1016/J.APGEOCHEM.2010.04.013

Pujo-Pay, M., Conan, P., Joux, F., Oriol, L., Naudin, J., Cauwet, G., 2006. Impact of phytoplankton and bacterial production on nutrient and DOM uptake in the Rhône River plume (NW Mediterranean). Marine Ecology Progress Series 315, 43–54. https://doi.org/10.3354/meps315043

Pujo-Pay, M., Conan, P., Oriol, L., Cornet-Barthaux, V., Falco, C., Ghiglione, J.-F., Goyet, C., Moutin, T., Prieur, L., 2011. Integrated survey of elemental stoichiometry (C, N, P) from the western to eastern Mediterranean Sea. Biogeosciences 8, 883–899. https://doi.org/10.5194/bg-8-883-2011

709 Pujo-Pay, M., Conan, P., Raimbault, P., 1997. Excretion of dissolved organic nitrogen by phytoplankton assessed by
710 wet oxidation and 15N tracer procedures. Marine Ecology Progress Series 153, 99–111.
711 https://doi.org/10.3354/meps153099

712 Pujo-Pay, M., Raimbault, P., 1994. Improvement of the wet-oxidation procedure for simultaneous determination of
713 particulate organic nitrogen and phosphorus collected on filters 105, 203–207.

714 Rodellas, V., Garcia-Orellana, J., Masque, P., Feldman, M., Weinstein, Y., 2015. Submarine groundwater discharge
715 as a major source of nutrients to the Mediterranean Sea. Proceedings of the National Academy of Sciences of
716 the United States of America 112, 3926–3930. https://doi.org/10.1073/pnas.1419049112

717 Rodellas, V., Garcia-Orellana, J., Tovar-Sánchez, A., Basterretxea, G., López-Garcia, J.M., Sánchez-Quiles, D.,
718 Garcia-Solsona, E., Masqué, P., 2014. Submarine groundwater discharge as a source of nutrients and trace
719 metals in a Mediterranean bay (Palma Beach, Balearic Islands). Marine Chemistry 160, 56–66.
720 https://doi.org/10.1016/J.MARCHEM.2014.01.007

721 Rodellas, V., Stieglitz, T.C., Andrisoa, A., Cook, P.G., Raimbault, P., Tamborski, J.J., van Beek, P., Radakovitch,
722 O., 2018. Groundwater-driven nutrient inputs to coastal lagoons: The relevance of lagoon water recirculation
723 as a conveyor of dissolved nutrients. Science of the Total Environment 642.
724 https://doi.org/10.1016/j.scitotenv.2018.06.095

725 Romey, C., Rochette, P., Vella, C., Arfib, B., Andrieu-Ponel, V., Braucher, R., Champollion, C., Douchet, M.,
726 Dussouillez, P., Hermitte, D., Mattioli, E., Parisot, J.-C., Schwenninger, J.-L., 2014. Geophysical and
727 geomorphological investigations of a Quaternary karstic paleolake and its underground marine connection in
728 Cassis (Bestouan, Cassis, SE France). Geomorphology 214, 402–415.
729 https://doi.org/10.1016/J.GEOMORPH.2014.02.021

730 Savriama, Y., Stige, L.C., Gerber, S., Pérez, T., Alibert, P., David, B., 2015. Impact of sewage pollution on two
731 species of sea urchins in the Mediterranean Sea (Cortiou, France): Radial asymmetry as a bioindicator of
732 stress. Ecological Indicators 54, 39–47. https://doi.org/10.1016/J.ECOLIND.2015.02.004

733 Slomp, C.P., van Cappellen, P., 2004. Nutrient inputs to the coastal ocean through submarine groundwater
734 discharge: controls and potential impact. Journal of Hydrology 295, 64–86.
735 https://doi.org/10.1016/j.jhydrol.2004.02.018

736 Sugimura, Y., Suzuki, Y., 1988. A high-temperature catalytic oxidation method for the determination of non-volatile
737 dissolved organic carbon in seawater by direct injection of a liquid sample. Marine Chemistry 24, 105–131.
738 https://doi.org/10.1016/0304-4203(88)90043-6

739 Sun, Y., Torgersen, T., 1998. The effects of water content and Mn-fiber surface conditions on 224Ra measurement
740 by 220Rn emanation. Marine Chemistry 62, 299–306. https://doi.org/10.1016/S0304-4203(98)00019-X

741 Tamborski, J., Beek, P., Rodellas, V., Monnin, C., Bergsma, E., Stieglitz, T., Heilbrun, C., Cochran, J.K.,
742 Charbonnier, C., Anschutz, P., Bejannin, S., Beck, A., 2019. Temporal variability of lagoon–sea water
743 exchange and seawater circulation through a Mediterranean barrier beach. Limnology and Oceanography
744 lno.11169. https://doi.org/10.1002/lno.11169

745 Tamborski, J., Bejannin, S., Garcia-Orellana, J., Souhaut, M., Charbonnier, C., Anschutz, P., Pujo-Pay, M., Conan,
746 P., Crispi, O., Monnin, C., Stieglitz, T., Rodellas, V., Andrisoa, A., Claude, C., van Beek, P., 2018. A
747 comparison between water circulation and terrestrially-driven dissolved silica fluxes to the Mediterranean Sea
748 traced using radium isotopes. Geochimica et Cosmochimica Acta 238, 496–515.
749 https://doi.org/10.1016/J.GCA.2018.07.022

750 Tovar-Sanchez, A., Basterretxea, G., Rodellas, V., Sanchez-Quiles, D., Garcia-Orellana, J., Masque, P., Jordi, A.,
751 Lopez, J.M., Garcia-Solsona, E., 2014. Contribution of Groundwater Discharge to the Coastal Dissolved
752 Nutrients and Trace Metal Concentrations in Majorca Island: Karstic vs Detrital Systems. Environmental
753 Science & Technology 48, 11819–11827. https://doi.org/10.1021/es502958t

754 Trezzi, G., Garcia-Orellana, J., Rodellas, V., Santos-Echeandia, J., Tovar-Sánchez, A., Garcia-Solsona, E., Masqué,
755 P., 2016. Submarine groundwater discharge: A significant source of dissolved trace metals to the North
756 Western Mediterranean Sea. Marine Chemistry 186, 90–100. https://doi.org/10.1016/j.marchem.2016.08.004

Twining, B.S., Baines, S.B., 2013. The Trace Metal Composition of Marine Phytoplankton. Annual Review of Marine Science 5, 191–215. https://doi.org/10.1146/annurev-marine-121211-172322

van Wambeke, F., Ghiglione, J.-F., Nedoma, J., Mével, G., Raimbault, P., 2009. Bottom up effects on bacterioplankton growth and composition during summer-autumn transition in the open NW Mediterranean Sea. Biogeosciences 6, 705–720. https://doi.org/10.5194/bg-6-705-2009

Wang, X., Li, H., Zheng, C., Yang, J., Zhang, Y., Zhang, M., Qi, Z., Xiao, K., Zhang, X., 2018. Submarine groundwater discharge as an important nutrient source influencing nutrient structure in coastal water of Daya Bay, China. Geochimica et Cosmochimica Acta 225, 52–65. https://doi.org/10.1016/J.GCA.2018.01.029

Windom, H.L., Moore, W.S., Niencheski, L.F.H., Jahnke, R.A., 2006. Submarine groundwater discharge: A large, previously unrecognized source of dissolved iron to the South Atlantic Ocean. Marine Chemistry 102, 252–266. https://doi.org/10.1016/J.MARCHEM.2006.06.016

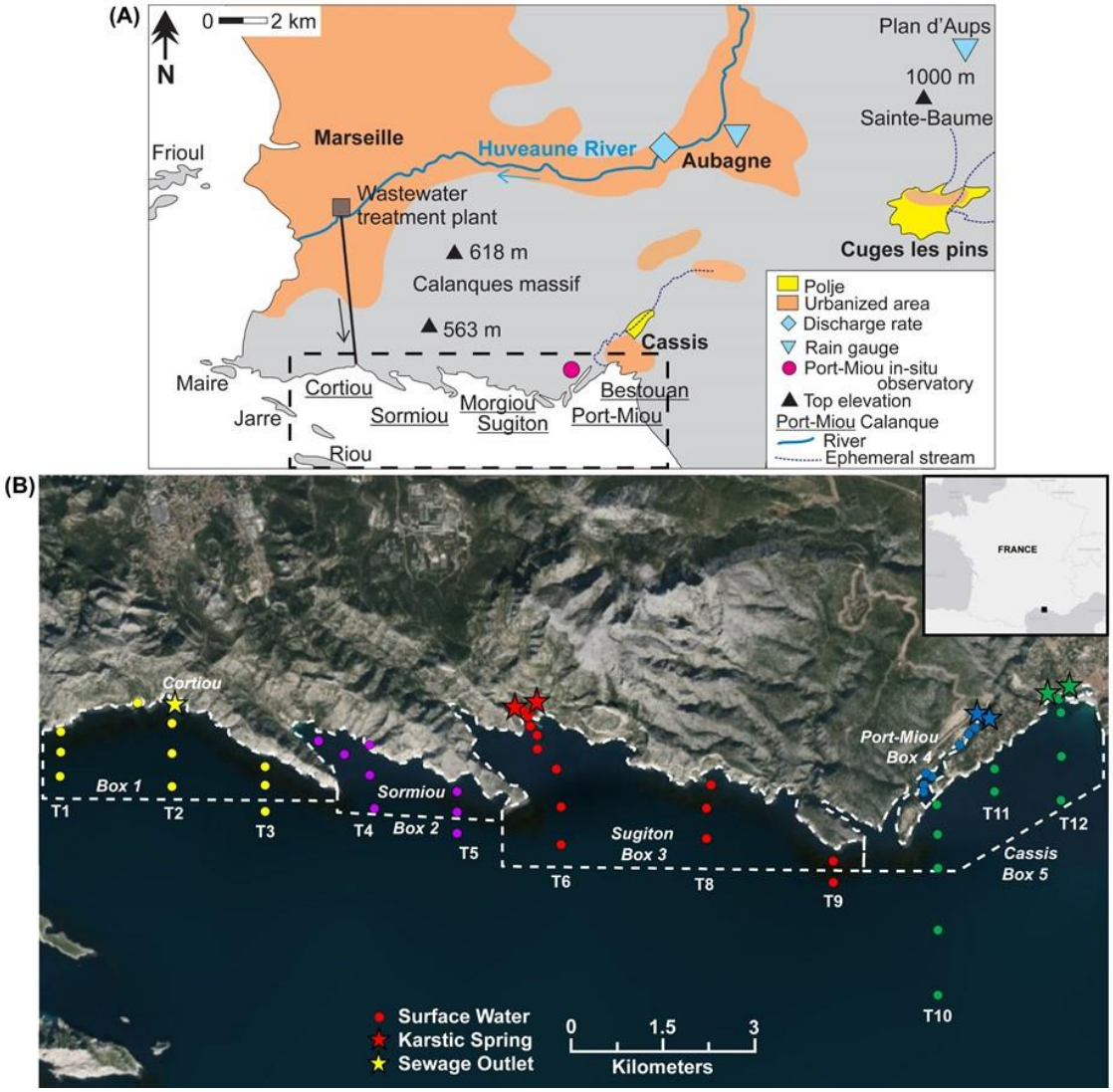

Figure 1. The Calanques of Marseille-Cassis (A), situated along the French Mediterranean coastline (B, inset black square). The black dashed rectangle in (A) corresponds to the location of subset panel (B). Surface water (circle), karstic groundwater (red, blue and green stars) and sewage effluent (yellow star) sampling stations are shown for the period 27th – 29th March, 2018. Transect labels (T1 – T12) are listed below each respective transect; note there is no T7.

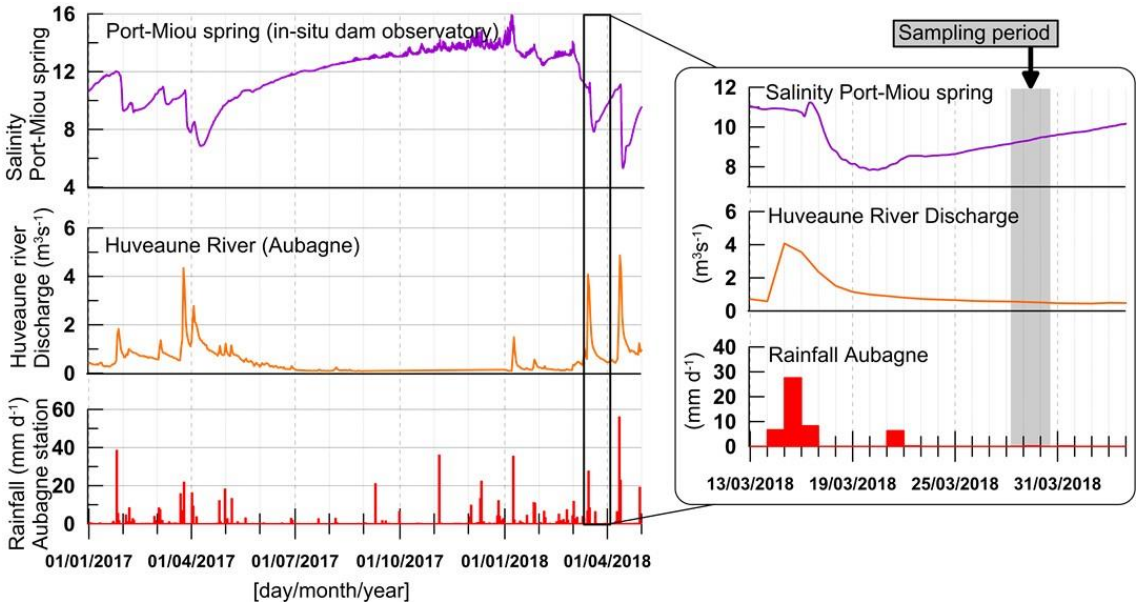

Figure 2. Port-Miou groundwater spring salinity (top) measured at the Port-Miou *in-situ* observatory, Huveaune River daily discharge (middle) measured at the Aubagne station upstream of Marseille and daily rainfall (bottom) from the nearby Aubagne station (Lat: 43.30667, Lon: 5.60000, z = 130 m; Figure 1A). Left panel: Long time-series (17 months). Right panel: Time-series of the two weeks preceding the sampling period (salinity recorded at 15-minute time-steps, average daily discharge); the sampling period of this study is indicated by a light-gray rectangle.

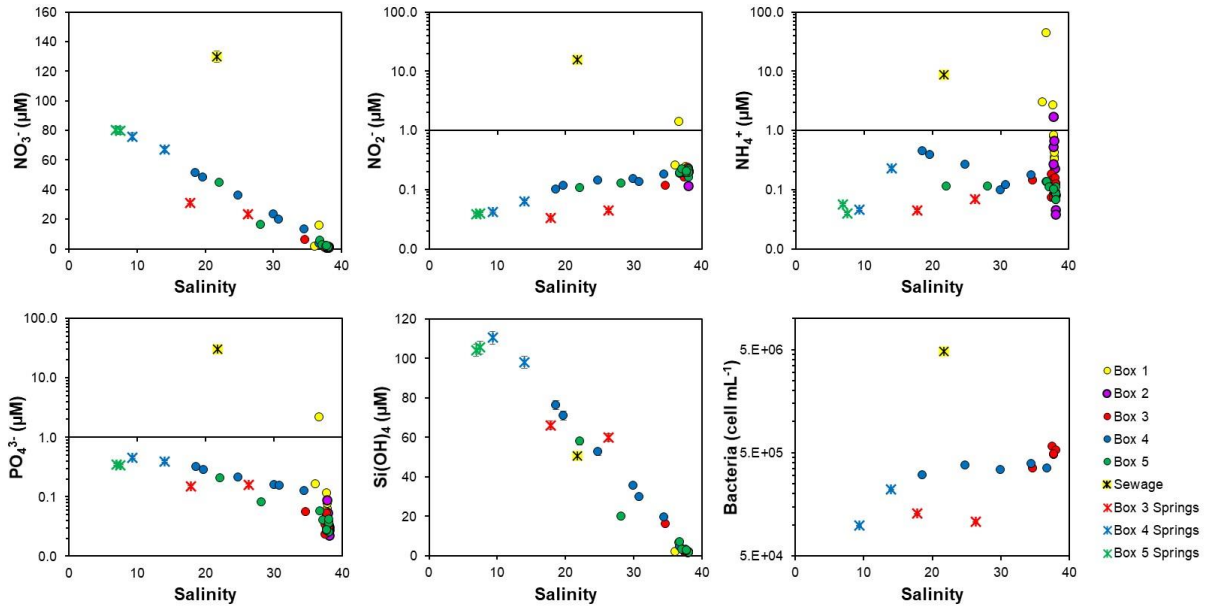

Figure 3. Major nutrient concentration and bacterial biomass versus salinity for coastal surface waters (circles), karstic springs (crosses) and water samples collected at the outlet of the Cortiou sewage outlet (yellow cross) on 27th – 29th March, 2018. Note the y-axes for NO_2^-, NH_4^+, PO_4^{3-} and bacterial biomass are log-scale. Only select samples were analyzed for bacterial biomass.

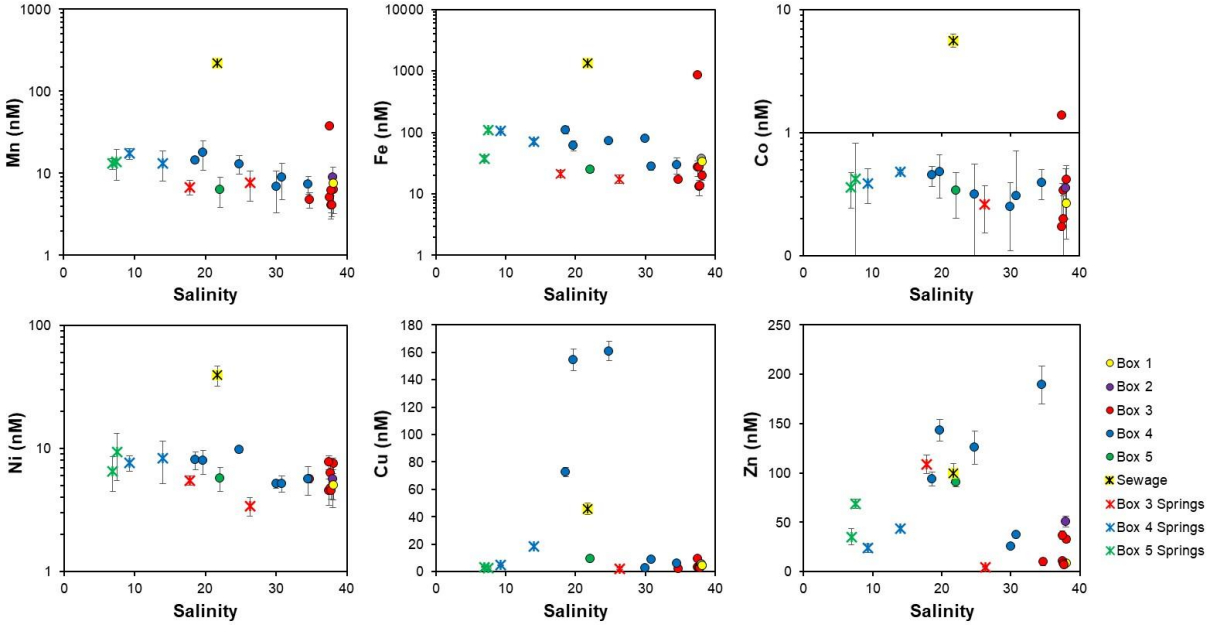

Figure 4. Trace element concentration versus salinity for select coastal surface waters (circles), karstic springs (crosses) and water samples collected at the outlet of the Cortiou sewage outlet (yellow cross) on 27th – 29th March, 2018. Note that the y-axes for Mn, Fe, Co and Ni are log-scale.

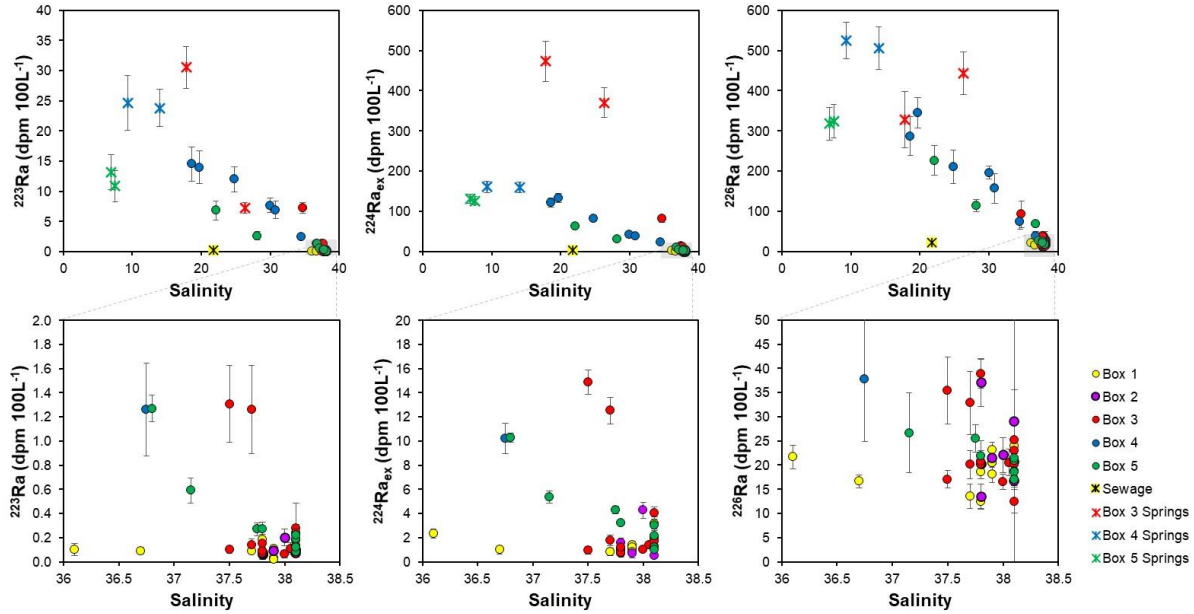

Figure 5. Ra isotope activity versus salinity for coastal surface waters (circles), karstic springs (crosses) and water samples collected at the outlet of the Cortiou sewage outlet (yellow cross) on 27th – 29th March, 2018. The lower panels represent the area of the gray rectangle of the above panel.

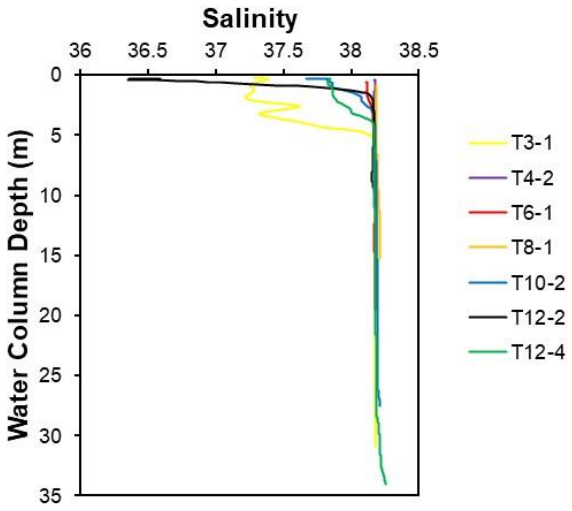

Figure 6. Select salinity profiles of the Calanques of Marseille-Cassis. Transect locations are shown on Figure 1; the second number corresponds to the offshore sample position for each respective transect. T3-1 = box 1, T4-2 = box 2, T6-1 & T8-1 = box 3, T10-2 = box 4/5 boundary, T12-2 & T12-4 = box 5.

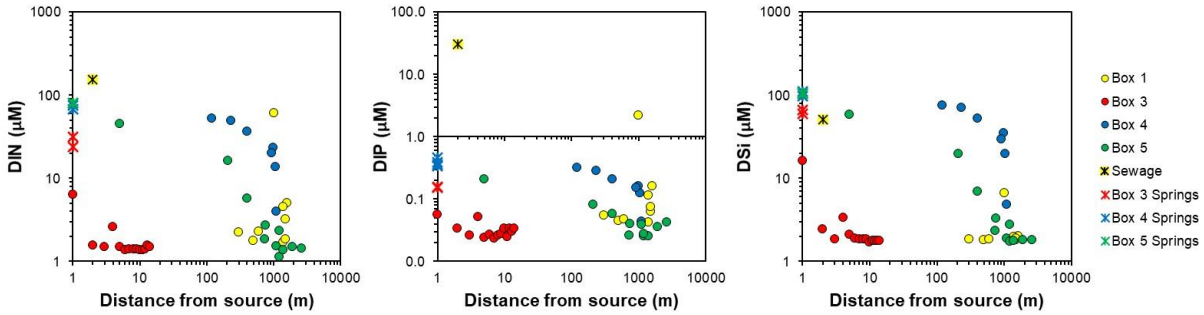

Figure 7. Surface water nutrient concentrations as a function of distance from a known point-source (sewage outlet or karstic spring). Only select stations are shown, in which the surface water sampling locations distance to the nearest known point-source could be well-defined; as a result, no stations are included for Box 2. Distances were measured using high resolution visible light imagery in Google Earth and assume a 20% measurement uncertainty. DIN = NO_2^- + NO_3^- + NH_4^+; DIP = PO_4^{3-}; DSi = $Si(OH)_4$.

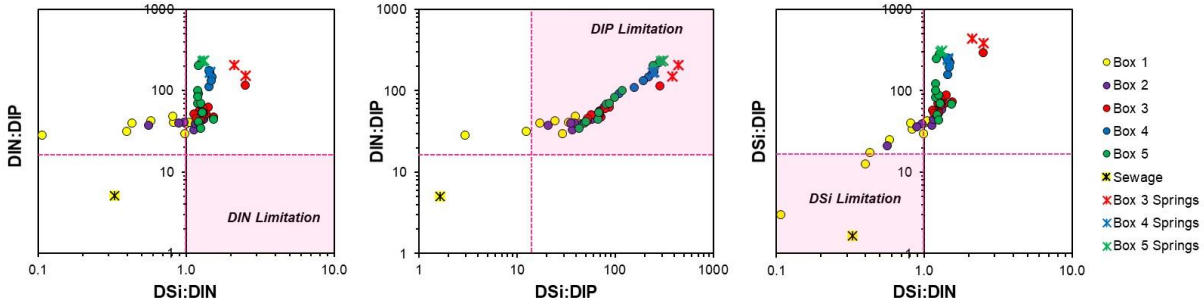

Figure 8. Relationships between stoichiometric ratios of DIN:DIP, DSi:DIN and DSi:DIP. Nutrient limitation is indicated by a shaded pink box for DIN (A), DIP (B) and DSi (C). DIN = NO_2^- + NO_3^- + NH_4^+; DIP = PO_4^{3-}; DSi = $Si(OH)_4$.

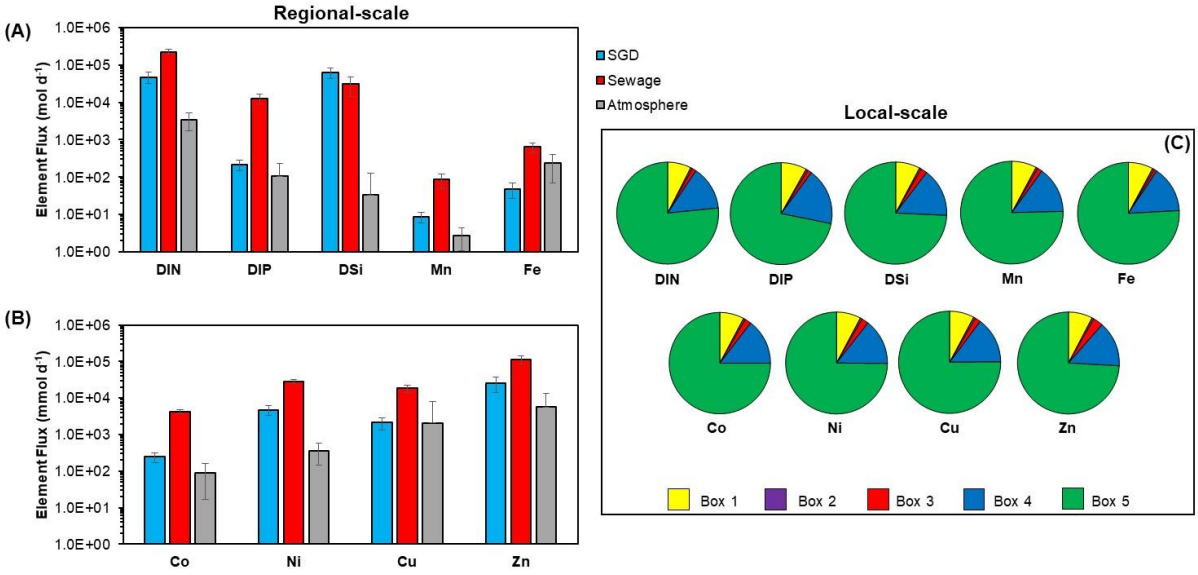

Figure 9. Comparison between chemical element fluxes from SGD (during 27th – 29th March, 2018), sewage effluent and atmospheric deposition to the entire shoreline of the Calanques of Marseille-Cassis. Note that regional fluxes in the upper panel (A) are reported in mol d^{-1} and in the lower panel (B) fluxes are reported in mmol d^{-1}. Pie charts (C) represent SGD-driven solute fluxes to each coastal box (local-scale). DIN = $NO_2^- + NO_3^- + NH_4^+$; DIP = PO_4^{3-}; DSi = $Si(OH)_4$.

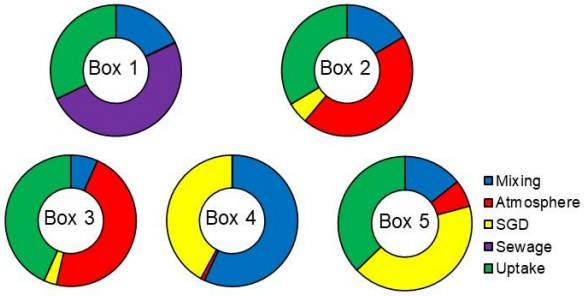

Figure 10. Summary of the coastal surface water DIP (PO_4^{3-}) budget during the study period, expressed as a percentage (Eq. 3) and arranged by box. Note that atmospheric inputs to Box 1 < 1%.

827 Table 1

828 Endmember nutrient and ancillary parameters summary for the karstic springs and Cortiou sewage effluent on 27th
829 – 29thMarch 2018. Box 3=Calanque of Sugiton; Box 4=Calanque of Port-Miou; Box 5 = Calanque of Cassis. (A)
830 and (B) refer to individual samples from two separate springs sampled within each box. BDL= below detection
831 limit.

ID	Latitude	Longitude	Salinity	pH	NO_3^-	NO_2^-	NH_4^+	PO_4^{3-}	$Si(OH)_4$	DIN/DIP
					µM	µM	µM	µM	µM	
Sewage outlet	43.212990	5.403210	21.7	7.31	130	16	9	31	51	5
Box 3(A)	43.211949	5.454708	26.3	7.57	24	0.05	0.07	0.16	60	152
Box 3 (B)	43.211784	5.455294	17.8	7.40	31	BDL	0.05	0.15	66	208
Box 4 (A)	43.211110	5.521090	9.3	7.07	76	BDL	0.05	0.46	110	167
Box 4 (B)	43.211140	5.521210	14.0	7.16	67	0.06	0.23	0.39	98	171
Box 5 (A)	43.213630	5.532860	7.5	7.03	80	BDL	0.04	0.34	105	235
Box 5 (B)	43.213953	5.533764	6.9	7.04	81	BDL	0.06	0.35	104	228

832

833

834

835 Table 2
836 Endmember bacterial biomass, particulate and dissolved organic nutrient summary for the karstic springs
837 and Cortiou sewage effluent on 27th – 29th March 2018. Box 3= Calanque of Sugiton; Box 4= Calanque of
838 Port-Miou. (A) and (B) refer to individual samples from two separate springs sampled within each box. Note
839 samples were not analyzed from box 5.

ID	Bacterial Biomass	DOC	POC	DON	PON	DOP
	$*10^5$ cell mL^{-1}	µM	µM	µM	µM	µM
Sewage outlet*	48.3	503	201	840	27	BDL
Box 3 (A)	1.07	61	2.3	0.14	0.24	0.13
Box 3 (B)	1.28	30	2.8	2.04	0.28	0.10
Box 4 (A)	0.99	85	1.1	13.7	0.12	0.08
Box 4 (B)	2.20	40	5.9	12.7	0.69	BDL

840

841 Table 3
842 Endmember trace element summary for the karstic springs and Cortiou sewage effluent on 27th – 29thMarch
843 2018. Box 3=Calanque of Sugiton; Box 4=Calanque of Port-Miou; Box 5 = Calanque of Cassis. (A) and (B) refer
844 to individual samples from two separate springs sampled within each box.

ID	Mn	Fe	Co	Ni	Cu	Zn
	nM	nM	nM	nM	nM	nM
Sewage effluent	221	1361	5.6	39	46	100
Box 3 (A)	8	17	0.3	3	2	5
Box 3 (B)	7	21	n/a	6	n/a	109
Box 4 (A)	17	107	0.4	8	5	24
Box 4 (B)	13	71	0.5	8	18	44
Box 5 (A)	14	109	0.4	9	3	69
Box 5 (B)	13	38	0.4	7	3	35

845

846

Table 4
Endmember Ra isotope summary for the karstic springs and Cortiou sewage effluent on 27th – 29th March 2018. Box 3 = Calanque of Sugiton; Box 4 = Calanque of Port-Miou; Box 5 = Calanque of Cassis. (A) and (B) refer to individual samples from two separate springs sampled within each box.

ID	^{223}Ra	$^{224}Ra_{ex}$	^{226}Ra
	dpm 100 L^{-1}	dpm 100 L^{-1}	dpm 100 L^{-1}
Sewage effluent	0.2 ± 0.1	3 ± 1	23 ± 7
Box 3 (A)	7 ± 1	370 ± 37	444 ± 53
Box 3 (B)	31 ± 3	473 ± 50	328 ± 70
Box 4 (A)	25 ± 4	161 ± 15	525 ± 45
Box 4 (B)	24 ± 3	159 ± 13	506 ± 53
Box 5 (A)	11 ± 3	126 ± 11	324 ± 41
Box 5 (B)	13 ± 3	132 ± 11	318 ± 41

Table 5
Parameters used in the simultaneous 224Raex and 226Ramass balances, arranged by coastal box (see Fig. 1). The 224,226Ra endmember of open seawater (224Rasea=1.0±0.2 dpm100 L−1; 226Rasea=15 ±2 dpm100 L−1; salinity = 37.9 ± 0.1; n = 3) is used to determine an excess 224Ra and 226Ra inventory supplied to each box by SGD.

Box #	Salinity	Area	Impacted depth	$^{224}Ra_{ex\text{-}box}$	$^{226}Ra_{box}$	Residence time	SGD
		m^2	m	dpm 100 L^{-1}	dpm 100 L^{-1}	d	m^3 s^{-1}
1	37.8 ± 0.5	5.43E+06	2.0	1.3 ± 0.6	16 ± 4	0.8 ± 0.4	0.52 ± 0.19[a]
2	37.9 ± 0.1	2.62E+06	1.0	1.0 ± 0.5	21 ± 5	12 ± 5	0.04 ± 0.01
3	37.9 ± 0.2	9.43E+06	3.5	1.2 ± 1.9	23 ± 5	39 ± 16	0.21 ± 0.05[b]
4	31.5 ± 5.0	2.11E+05	1.0	38 ± 31	155 ± 78	0.6 ± 0.3	0.97 ± 0.34[c]
5	37.0 ± 2.4	5.39E+06	4.0	5.3 ± 7.4	33 ± 15	2.1 ± 1.0	4.97 ± 1.96[d]
Sum		2.31E+07					6.7 ± 2.0

[a] SGD into box 1 is corrected for 226Ra inputs from sewage outfall.
[b] Using an average Ra isotope endmember (from boxes 4 and 5) for box 3 results in a residence time and SGD flow of 11.6 d and 0.7 m^3 s^{-1}.
[c] SGD into box 4 only includes surficial springs.
[d] SGD into box 5 inc ludes the main submerged Port-Miou spring that is located near the boundary of boxes 4 and 5 (see Section 3.4 for further clarification).